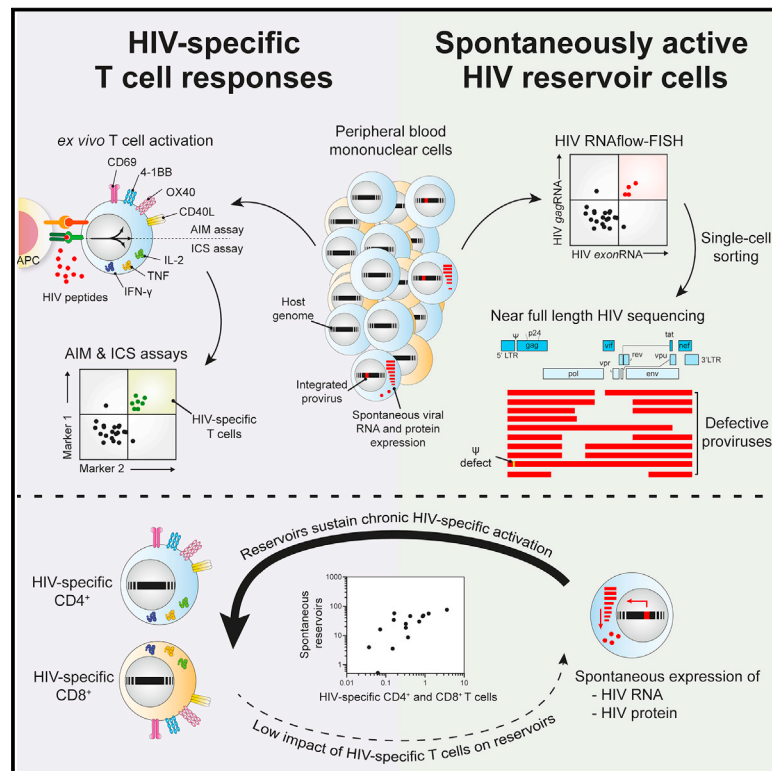


Cell Host & Microbe

Spontaneous HIV expression during suppressive ART is associated with the magnitude and function of HIV-specific CD4⁺ and CD8⁺ T cells

Graphical abstract



Authors

Mathieu Dubé, Olivier Tastet, Caroline Dufour, ..., Rémi Fromentin, Nicolas Chomont, Daniel E. Kaufmann

Correspondence

mathieu.dube.chum@ssss.gouv.qc.ca (M.D.),
daniel.kaufmann@chuv.ch (D.E.K.)

In brief

Dubé et al. identify phenotypically diverse HIV-infected cells that spontaneously express viral RNA, and occasionally protein, during antiretroviral treatment. Despite carrying defective proviruses, active reservoirs correlate with HIV-specific CD4⁺ and CD8⁺ T cell responses. These results suggest that ongoing expression of viral genes maintain HIV-specific immune responses during suppressive ART.

Highlights

- Spontaneously active HIV RNA⁺ and protein^{+/-} reservoirs exist in people with HIV on ART
- These are enriched in central memory and CCR6⁻ and activation-marker-expressing cells
- Proviruses integrated in these active reservoir cells are mostly defective
- Spontaneously active reservoirs correlate with HIV-specific CD4⁺ and CD8⁺ T cells



Article

Spontaneous HIV expression during suppressive ART is associated with the magnitude and function of HIV-specific CD4⁺ and CD8⁺ T cells

Mathieu Dubé,^{1,*} Olivier Tastet,¹ Caroline Dufour,^{1,2} Gérémy Sannier,^{1,2} Nathalie Brassard,¹ Gloria-Gabrielle Delgado,¹ Amélie Pagliuzza,¹ Corentin Richard,¹ Manon Nayrac,¹ Jean-Pierre Routy,^{3,4} Alexandre Prat,^{1,5} Jacob D. Estes,^{6,7} Rémi Fromentin,¹ Nicolas Chomont,^{1,2} and Daniel E. Kaufmann^{1,2,8,9,*}

¹Department of Immunopathology, Research Centre of the Centre Hospitalier de l'Université de Montréal (CRCHUM), Montreal, QC H2X 0A9, Canada

²Department of Microbiology, Infectious Diseases and Immunology, Faculty of Medicine, Université de Montréal, Montreal, QC H3C 3J7, Canada

³Chronic Viral Illnesses Service and Division of Hematology, McGill University Health Centre (CUSM), Montreal, QC H4A 3J1, Canada

⁴Infectious Diseases and Immunity in Global Health Program, Research Institute, McGill University Health Centre, Montreal, QC H4A 3J1, Canada

⁵Department of Neurosciences, Faculty of Medicine, Université de Montréal, Montréal, QC H3C 3J7, Canada

⁶Vaccine and Gene Therapy Institute, Oregon Health & Science University, Beaverton, OR 97006, USA

⁷Oregon National Primate Research Center, Oregon Health & Science University, Beaverton, OR 97006, USA

⁸Division of Infectious Diseases, Department of Medicine, Lausanne University Hospital and University of Lausanne, 1011 Lausanne, Switzerland

⁹Lead contact

*Correspondence: mathieu.dube.chum@ssss.gouv.qc.ca (M.D.), daniel.kaufmann@chuv.ch (D.E.K.)

<https://doi.org/10.1016/j.chom.2023.08.006>

SUMMARY

Spontaneous transcription and translation of HIV can persist during suppressive antiretroviral therapy (ART). The quantity, phenotype, and biological relevance of this spontaneously “active” reservoir remain unclear. Using multiplexed single-cell RNAflow-fluorescence *in situ* hybridization (FISH), we detect active HIV transcription in 14/18 people with HIV on suppressive ART, with a median of 28/million CD4⁺ T cells. While these cells predominantly exhibit abortive transcription, p24-expressing cells are evident in 39% of participants. Phenotypically diverse, active reservoirs are enriched in central memory T cells and CCR6- and activation-marker-expressing cells. The magnitude of the active reservoir positively correlates with total HIV-specific CD4⁺ and CD8⁺ T cell responses and with multiple HIV-specific T cell clusters identified by unsupervised analysis. These associations are particularly strong with p24-expressing active reservoir cells. Single-cell vDNA sequencing shows that active reservoirs are largely dominated by defective proviruses. Our data suggest that these reservoirs maintain HIV-specific CD4⁺ and CD8⁺ T responses during suppressive ART.

INTRODUCTION

The persistence of HIV represents a fundamental challenge to achieving a cure. When antiretroviral therapy (ART) is interrupted in people with HIV (PWH), rare persisting infected cells can fuel viral rebound.¹ Recent advances provided sensitive evaluations of the size of the HIV reservoir.² CD4⁺ T cells bearing HIV genomes^{3,4} are one order of magnitude more abundant than those with the ability to transcribe multiply spliced RNA,^{5,6} themselves another order of magnitude more frequent than those producing p24.^{7–9} These differences may reflect stepwise stages of blocks in viral transcription and translation.^{10,11} Detecting viral reservoirs based on either viral RNA (vRNA) or protein typically involves *ex vivo* stimulation with latency reversal agents (LRAs) that induce viral gene expression. This approach provided valuable information on inducible reservoirs poised for reactivation.

Current antiretroviral therapies do not target HIV transcription nor translation; therefore, spontaneous viral gene transcription^{10,12–17} and translation^{18–20} can persist during ART. The definite quantification, single-cell phenotyping, and biological relevance of these “active” reservoir cells are not established.

CD4⁺ and CD8⁺ T cells are increasingly recognized as essential actors in the control of simian immunodeficiency virus (SIV) and HIV infections.^{21–26} Consequently, anti-HIV immunity is expected to play an important role in cure strategies and to contribute to purging reservoirs, exerting immunosurveillance of residual virus and/or supporting the development of broadly neutralizing HIV-specific antibodies.^{27,28} HIV-specific CD4⁺ and CD8⁺ T cells can be detected during ART, although their magnitude and functions present notable interindividual heterogeneity.^{29–32} The mechanisms involved in the persistence of such HIV-specific immunity during suppressive ART are not



entirely understood but are unlikely to result from ongoing residual viral replication, an actively debated concept.^{33–36} Conversely, active reservoirs that lead to protein expression from a fraction of the largely dominant pool of defective proviruses and low-level virion release from an even smaller proportion of active reservoirs with intact genomes could maintain and shape anti-HIV CD4⁺ and CD8⁺ T cell responses during ART.^{14,37–40}

Herein, we quantified and phenotyped viral reservoirs spontaneously expressing vRNA and the p24 protein in primary clinical samples directly *ex vivo*. We found associations between active reservoirs and HIV-specific CD4⁺ and CD8⁺ T cells, supporting that low-level viral gene expression by spontaneous reservoirs is sufficient to maintain anti-HIV adaptive immunity.

RESULTS

Spontaneous vRNA-expressing reservoirs are detectable in a majority of ART-suppressed PWH

We previously used a multiplexed HIV RNAflow-fluorescence *in situ* hybridization (FISH) assay to characterize viral reservoirs induced *ex vivo*.^{7–9} A previous digital-droplet study on bulk CD4⁺ T cells showed expression during latency of “long-LTR” abortive transcripts.^{10,41} Therefore, to maximize detection of viral reservoir cells that spontaneously express vRNA without *ex vivo* stimulation, termed active reservoir, we adapted our multiplexed vRNA detection strategy and focused on 5′ HIV genes (Figure 1A). As described before,⁹ a first-step analysis provided an inclusive detection of viral transcripts, consisting of an *exonRNA* probe set targeting exon sequences, including a portion of the 5′ long terminal repeat (LTR) region, present on all viral transcripts.⁴² The second step of detection added stringency and ensured specificity. To this end, two additional probe sets were generated: (1) a *gagRNA* probe set, detecting full-length genomic transcripts but also shorter abortive or defective transcripts containing at least a portion of the *gag* gene,⁹ and (2) a *polRNA* detecting transcripts that elongated beyond the gene *gag*. We also stained intracellular p24 to assess viral translation.

We used this adapted HIV RNAflow assay to quantify the viral reservoirs in 18 PWH on ART for >3 years (median = 10 years, see clinical characteristics in Table S1). To reveal inducible viral reservoirs, CD4⁺ T cells isolated from peripheral blood mononuclear cells (PBMCs) were treated 15 h with phorbol myristate acetate (PMA)/ionomycin. To identify viral reservoirs that are able to spontaneously express HIV RNA and/or protein, we left CD4⁺ T cells unstimulated after isolation. We identified HIV-infected cells by Boolean ORgating⁹ and therefore included any cells either *exonRNA*⁺*gagRNA*⁺ or *exonRNA*⁺*polRNA*⁺ or *exonRNA*⁺*p24*⁺ into a single non-overlapping population expressing any combination of the viral genes assessed (henceforth termed vRNA⁺; Figure S1A). CD4⁺ T cells from 6 uninfected donors (UDs) served as specificity controls. We set a positive detection threshold at 7 events/10⁶ CD4⁺ T cells corresponding to the mean detection in UD plus twice the standard deviation, rounded up (mean + 2SD). Based on these criteria, we detected spontaneous reservoirs in 78% (14/18) of PWH on suppressive ART, with a median of 28 active vRNA⁺ cells/10⁶ CD4⁺ (Figure 1B). This level of detection represents a compromise compared to limiting dilution assays with quantitative reverse transcription po-

lymerase chain reaction (RT-qPCR), sacrificing some sensitivity for higher throughput and the ability to maintain phenotyping capability (Figures S1F and S1G). PMA/ionomycin-inducible reservoirs could be detected in 89% (16/18) of participants, with a significantly higher median (79 vRNA⁺/10⁶ CD4⁺). Reservoirs induced by Panobinostat and ingenol-3-angelate (termed LRA) reached an even higher level (325 induced vRNA⁺/10⁶ CD4⁺) (Figure S1B). By comparison, the frequency of CD4⁺ T cells harboring integrated HIV DNA was 12-fold higher than PMA/ionomycin-inducible reservoirs. In contrast, inducible reservoirs were 3-fold more frequent than spontaneous reservoirs (Figure 1C). We calculated that a median of 10% of the CD4⁺ T cells harboring integrated HIV DNA produced viral transcripts upon stimulation, whereas 4% spontaneously expressed vRNA (Figure 1D). Active vRNA⁺ reservoirs correlated with total and integrated HIV DNA (Figures 1E and 1F), whereas PMA/ionomycin-induced reservoirs showed strong trends (Figures S1C and S1D). We found strong associations between reservoir cells with spontaneous viral expression and both PMA/ionomycin (Figure 1G) and LRA-inducible (Figure S1E) reservoirs.

We next tested for associations between integrated HIV DNA, inducible and spontaneously active vRNA⁺ reservoirs, and clinical features (Figure 1H). The time of infection correlated with the size of inducible reservoirs, with a positive trend with the magnitude of the spontaneous reservoir. There was no association between the spontaneous reservoir and time on ART, while there was an association for inducible reservoirs. The level of spontaneous vRNA expression, but not inducibility, was associated with a longer duration of untreated infection. CD4⁺ T cell counts, CD4/CD8 ratios and pre-ART viral loads did not correlate with either inducible or spontaneous reservoirs.

Globally, these data highlighted the existence of spontaneous vRNA⁺ reservoirs in most PWH on suppressive ART. Spontaneous and inducible reservoirs were strongly associated, suggesting a robust relationship.

Spontaneously active reservoirs are enriched in short abortive and defective *gagRNA*⁺ transcripts

We next sought to characterize these active reservoirs based on p24 (Figure 2A), *gagRNA*, and *polRNA* co-expression (Figure 2B). The expression of p24 was used to assess viral protein expression,^{8,9} whereas *gagRNA* and *polRNA* defined the processivity of the transcription. This bilayered analysis created 8 theoretical subpopulations (Figures 2C, S2A, and S2B). Among these, single *exonRNA*⁺ cells could not be interpreted because of the insufficient specificity of single-parameter detection.⁹ The prevalence of the remaining seven theoretical populations is summarized in Figures 2D and S2A. Unstimulated samples from ART-suppressed individuals were homogeneously enriched in p24[−]*gagRNA*⁺*polRNA*[−] cells (Figure S2C). This population corresponded to short abortive or deleted transcripts (*gagRNA*⁺) described before.^{9,10} PMA/ionomycin-induced reservoirs presented a more heterogeneous profile: although p24[−]*gagRNA*⁺*polRNA*[−] cells were frequent, other more processive populations could also be detected, such as p24[−]*gagRNA*⁺*polRNA*⁺ (elongated transcripts not sustaining translation, termed vRNA_{DP} for “double *gagRNA*⁺*polRNA*⁺ positive”) > p24[−]*gagRNA*[−]*polRNA*⁺ (likely deleted transcripts, termed *polRNA*⁺) > p24⁺*gagRNA*⁺*polRNA*⁺ (translation-competent reservoirs, termed p24⁺). The

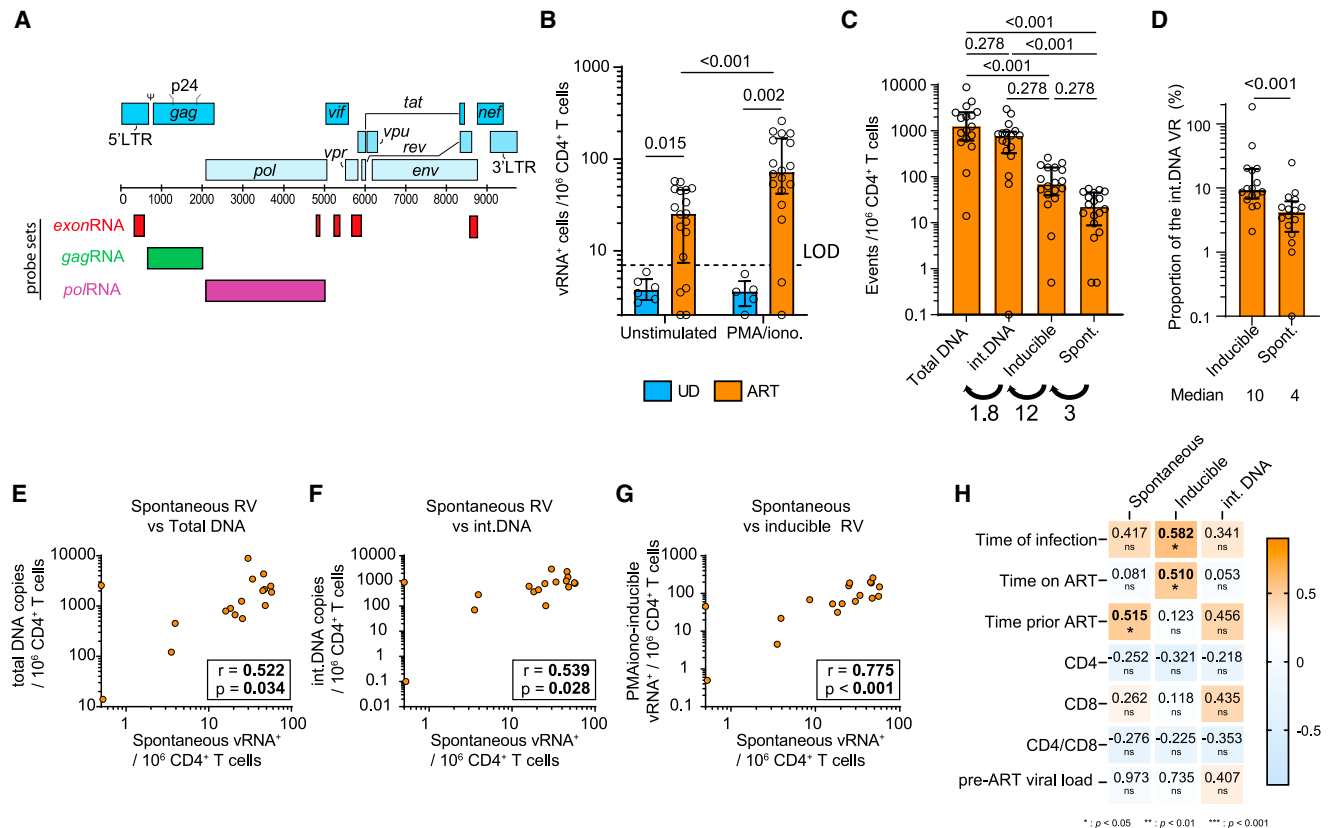


Figure 1. Spontaneous vRNA expression by HIV reservoirs in ART-suppressed PWH

(A) vRNA probe set designs.

(B) Quantification of vRNA⁺ cells in purified CD4⁺ T cells from ART-treated PWH and uninfected (UD) as controls. Cells were either unstimulated or treated *ex vivo* with PMA/ionomycin for 15 h. Two statistical tests are shown: Mann-Whitney for cohort comparisons and Wilcoxon between stimulations.

(C) Comparison between four different types of viral reservoir measurements. Numbers below indicate the median fold increase between groups.

(D) The proportion of inducible and spontaneous vRNA⁺ reservoirs using integrated DNA as denominator. A Wilcoxon test was performed, shown above. Median values are shown below.

(E–G) Correlations between (E) spontaneous reservoirs and total DNA, (F) spontaneous reservoirs and integrated DNA, (G) spontaneous and inducible reservoirs, with *r* and *p* values from Spearman tests.

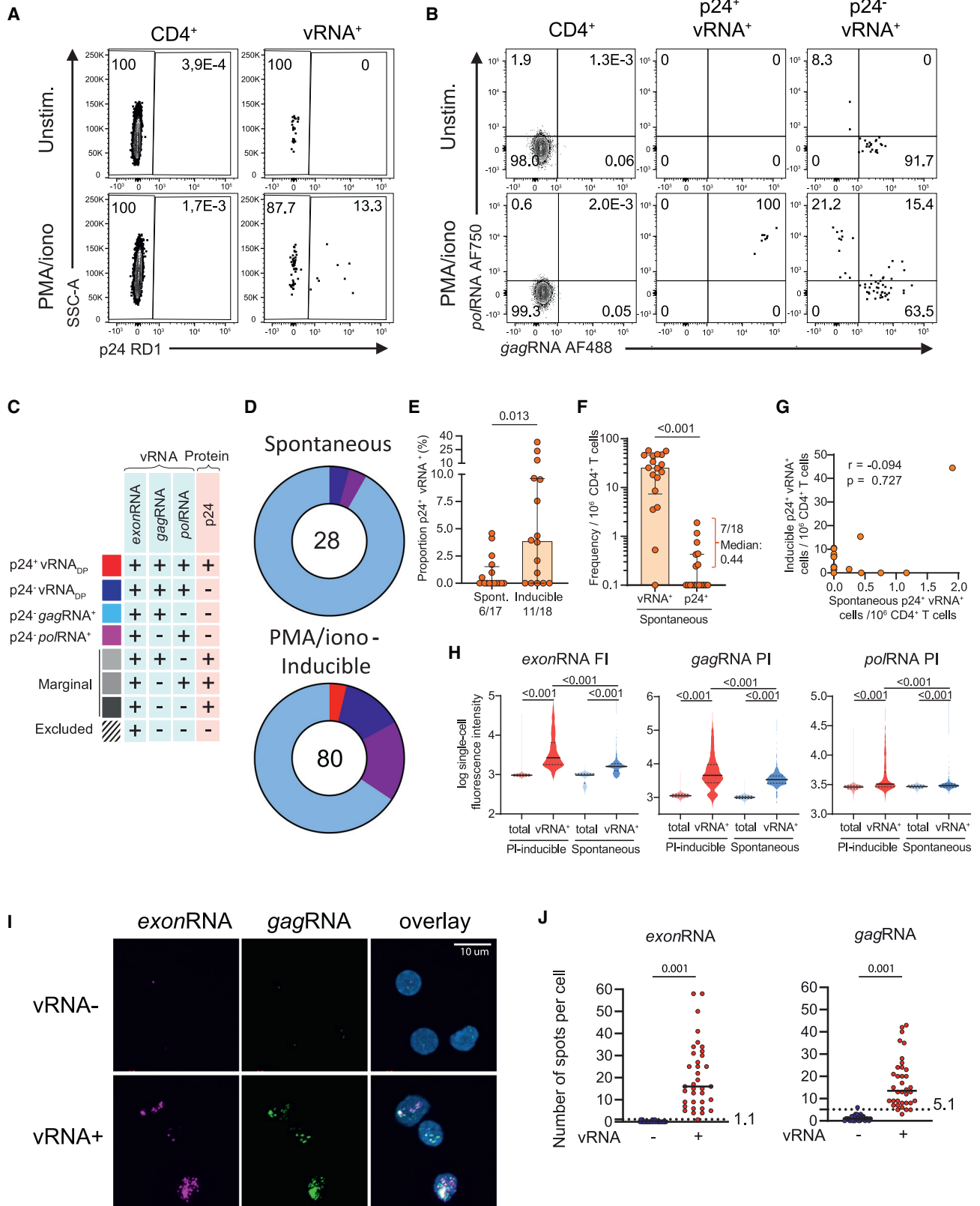
(H) Correlations between reservoir metrics and indicated clinical parameters. CD4 and CD8 stand for CD4⁺ and CD8⁺ T cell clinical counts. Values in the heatmap indicate *r* values, with *p* values underneath: **p* < 0.05, ***p* < 0.01, ****p* < 0.001. The shade of colors indicates the *r* value. Results reaching statistical significance are shown in bold. *n* = 18.

In (B) and (D), the histograms indicate the median, and the error bars illustrate the interquartile range.

pattern of active reservoirs was similar to combinatory LRA (Panobinostat + ingenol), with strong expression of *gag*RNA and little expression of *pol*RNA and marginal p24 translation (Figures S2A and S2C).^{9,10} In a subset of participants, the *pol*RNA probe set was substituted by a more distal *nef*RNA probe set.⁹ We detected rare *nef*RNA⁺ cells among active reservoirs and none that co-expressed *gag* and *nef* genes (Figure S2B), further suggesting unproductive transcription aborting in the 5' portion of the viral genome. Spontaneous p24-expressing cells represented a rare fraction (Figure 2E). These cells could be detected at low frequencies in 7/18 HIV⁺ participants, with a median frequency of 0.44 p24⁺vRNA⁺ cell/10⁶ CD4⁺ (Figure 2F). These active p24⁺ cells did not correlate with translation-competent reservoirs identified after PMA/ionomycin-stimulation (Figure 2G).

We used cytometric fluorescent intensities (FIs) to obtain a semi-quantitative measurement of RNA copies/cell⁴³ and as-

sessed the viral transcription and translation levels/infected cell. We used this metric to determine whether the level of viral transcription could define the success of viral translation. To avoid biases due to a low number of viral reservoir cells in some PWH, we concatenated all events per condition. Since *exon*RNA is expressed in all vRNA⁺ cells, we used it as a surrogate of global transcriptional activity. In both PMA/ionomycin- or LRA-induced reservoirs, the single-cell *exon*RNA, *gag*RNA, and *pol*RNA expression presented a skewed distribution composed of a low-yield bulky population and a tail spreading about one order of magnitude higher (Figures 2H and S2E). p24-expressing PMA/ionomycin-induced vRNA⁺ cells were almost exclusively found in these tails of high v transcriptional activity (Figure S2F). Consistent with the rare p24 expression in active reservoirs, such a high-yield tail was essentially absent in spontaneous reservoirs. Instead, *exon*RNA and *gag*RNA could be detected at low levels, whereas *pol*RNA expression remained comparably



(legend on next page)

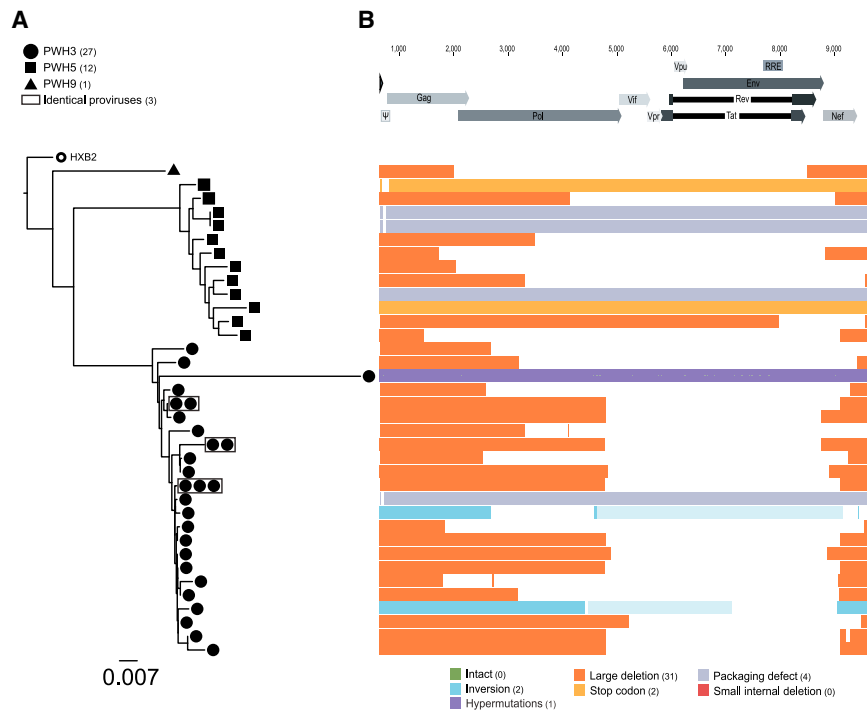


Figure 3. Near full-length single-cell vDNA sequencing of spontaneously active viral reservoirs identifies underlying proviral defects

Purified CD4⁺ T cells from 3 ART-treated participants were co-stained by multiplexed HIV-1 RNAflow-FISH. vRNA⁺ cells were individually sorted for nested PCR amplification and near full-length sequencing.

(A) Phylogenetic trees for the three participants PWH3, PWH5, and PWH9 built from the entire amplified area sequenced based on maximum likelihood. Sequences with 100% identity are boxed in gray.

(B) List of the different defects found in the 36 proviral sequences, aligned on the Hx2B2 genome. The type of defect is color coded, based on the legend presented below.

marginal (Figure 2H). In contrast to spontaneous p24⁺ cells, the levels of CD4 on the surface of spontaneous vRNA⁺ cells were comparable to vRNA⁻ cells, suggesting suboptimal or no expression of Nef and Vpu proteins (Figure S2G). These data demonstrate the low-yield, unprocessed nature of the active reservoirs.

We next used confocal fluorescence microscopy to count the number of HIV RNA foci per vRNA⁺ cell, as done previously.⁶ We sorted vRNA⁺ and vRNA⁻ cells, imaged and manually enumerated foci per cell (Figures S2H and 2I). The conservative false-positive rates (assuming Gaussian distribution, mean foci/cell in vRNA⁻ cells + 3SD) were established at 1.1 foci/cell for *exonRNA* and 5.1 foci/cell for *gagRNA* (Figure 2J). Conversely, vRNA⁺ cells containing down to 5 foci were clearly detected for both probes, but few vRNA⁺ cells were below this cutoff. The median detection reached 16 foci for *exonRNA* and 14 foci/cell for *gagRNA*, both significantly higher than their respective false-positive rate. *exonRNA*⁺ and *gagRNA*⁺ foci/cell corre-

lated significantly (Figure S2I). Taken together, these results suggest that our approach can reliably identify spontaneously active reservoirs with a cutoff of 5 vRNA copies/cell. To determine the proviral features of spontaneously vRNA⁺ cells, we next performed near full-length sequencing of using a modified full-length individual proviral sequencing (FLIPS) assay^{9,44} (Figure 3). We obtained a total of 40 amplicons from three ART-treated participants. From these 40 amplicons there was 36 distinct viral DNA (vDNA) sequences, and 3 small clones (Figure 3A). Most sequences harbored large deletions spanning the entire *env* region. Deletions in *pol* were also common (Figure 3B). We found two sequences with an inversion. Seven amplicons were near null length: one was hypermutated, two had early stop codons, and two bore packaging signal defects. No intact proviral sequence were found in our limited sampling. This indicates that spontaneous viral transcription is mainly fueled by defective proviruses.

Spontaneously active viral reservoirs are phenotypically diverse

LRA stimulation can alter cell surface marker expression, thus biasing phenotyping.⁹ As measuring spontaneously vRNA⁺ cells

Figure 2. Spontaneously active reservoirs are enriched in short vRNA transcripts

- (A and B) Gating strategy to assess: (A) p24 expression in vRNA⁺ cells and (B) *gagRNA* and *polRNA* co-expression in p24⁻ or p24⁺ vRNA⁺ cells.
 (C) List of the theoretical vRNA⁺ populations.
 (D) Donut charts presenting the median proportions of each vRNA⁺ subpopulation for spontaneous or PMA/ionomycin-induced reservoirs, as colored in (C). Numbers in the donut holes represent the median vRNA⁺/10⁶ CD4⁺.
 (E) The proportion of p24⁺ cells in spontaneous compared with PMA/ionomycin-induced vRNA⁺ reservoirs. The frequency of participants with p24⁺ cell detection is indicated underneath.
 (F) Compared frequencies of spontaneous vRNA⁺ and p24⁺ cells. The median of the 7 participants in which p24 was spontaneously detected is shown.
 (G) Correlation between p24⁺ cells in unstimulated and PMA/ionomycin-induced conditions.
 (H) Violin plots showing total single-cell fluorescence intensities in 18 participants.
 (E and F) The bars indicate the median. The error bars illustrate the interquartile range. Results from Wilcoxon tests are shown above. n = 18 (excepted for E, where n = 16 because <5 vRNA⁺ events were detected in two participants).
 (I) Representative maximal intensity of confocal microscopy projections from z stacks of vRNA⁻ and vRNA⁺ sorted cells. The scale is represented by the white bar (10 μm).
 (J) Number of spots per cell for *exonRNA* (left) and *gagRNA* (right) probes. The results from a Mann-Whitney test are shown above. False-positive rates are indicated by the dashed lines.

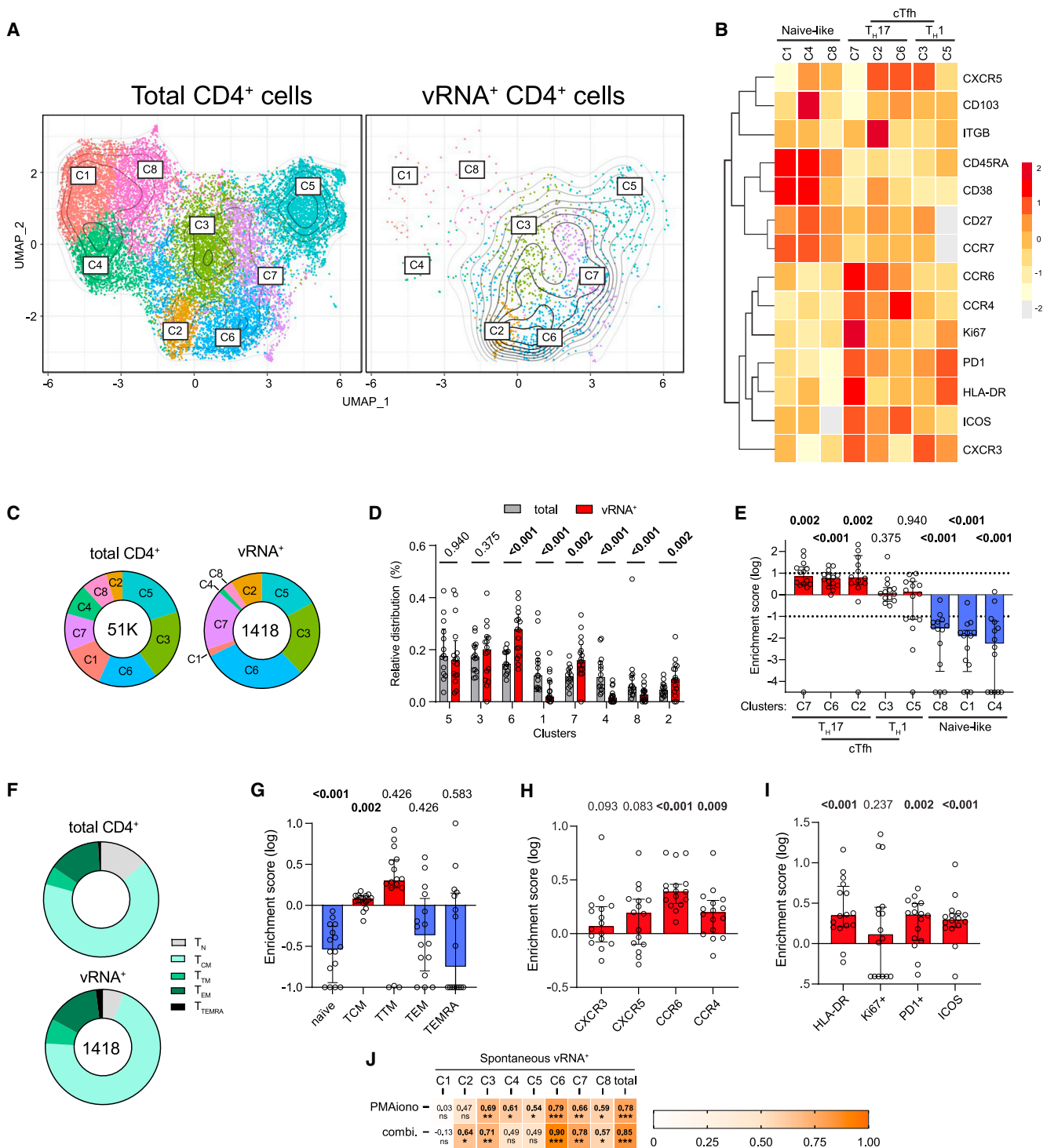


Figure 4. Spontaneously active viral reservoirs are phenotypically diverse

(A) Global uniform manifold approximation and projection (UMAP) for dimension reduction map of all 1,418 vRNA⁺ cells. These cells were embedded among downsampled 3,000 CD4⁺ per donor to help identify stable population clusters. All 8 clusters are identified. Individual CD4 (left) and vRNA⁺ (right) UMAP are shown. Contours show the density of vRNA⁺ cells.

(B) Heatmap showing an unsupervised hierarchical clustering of the 8 clusters, defined by MFI.

(C) The donut charts present the proportion of each cluster for the indicated population, with color matching with (A). The total number of events used to generate the plot are indicated in the donut holes.

(D) The histogram presents the proportion of each cluster, with a side-by-side comparison between CD4 and vRNA⁺ cells. Wilcoxon tests are shown.

(E) The enrichment score for each cluster is calculated as the log of the ratios between vRNA⁺/CD4 cluster proportions.

(legend continued on next page)

does not require an *in vitro* stimulation, the experimental approach used allows reliable phenotyping of viral reservoir cells. We performed unsupervised analyses of high-dimensional flow cytometric phenotyping data to avoid a priori-defined marker combinations (Figure 4). We examined features that were previously found enriched in HIV-infected cells either during ART or during untreated chronic infection (Table S2): chemokine receptors involved in tissue homing ([CXCR5 for Tfh, CXCR3 for Th1, CCR6 for Th17/Th22, and CCR4 for Th2, also expressed on Th17/Th22 and Tregs; reviewed in Strazza and Mor⁴⁵]; gut homing markers [integrin β 7 and CD103, reviewed in Barczyk et al.⁴⁶]; activation markers [CD38, HLA-DR, and ICOS]; cell cycle/proliferation [Ki67]; inhibitory checkpoint [PD-1]; and memory and differentiation markers [CD45RA, CCR7, and CD27]). To avoid excessive background noise in phenotype profiling, we focused the analyses on participants with >5 vRNA⁺ cells and with spontaneous reservoirs above the level of positivity (14/18 participants).

We illustrated the distribution of clustered populations by the uniform manifold approximation and projection (UMAP) algorithm.⁴⁷ To help define clear phenotypic clusters, all identified vRNA⁺ cells were concatenated and downsampled to 3,000 autologous CD4⁺ T cells per participant. Cluster identification was performed using PhenoGraph.⁴⁸ 8 clusters were defined based on distinct profiles of relative marker expression (Figures 4A and 4B and S3A). Active vRNA⁺ reservoir cells were found in all 8 clusters (Figures 4C and 4D). However, compared with total CD4⁺ T cells, vRNA⁺ cells were sparsely found in clusters C1, C4, and C8 (Figures 4A, 4C, and 4D) enriched in CD45RA, CCR7, and CD27, consistent with a naive phenotype (Figure 4B). CCR7 and CD27 expression was moderate in CD45RA-negative clusters C2, C3, C5, C6, and C7, suggesting that these clusters are composed of mixed populations of central memory (T_{CM}), transitional memory (T_{TM}), and effector memory (T_{EM}) cells defined by other phenotypic markers (Figure 4B). We calculated enrichment scores to evaluate the relative over- or under-representation of active vRNA⁺ reservoir cells among the identified clusters (Figure 4E). This analysis confirmed the under-representation of active vRNA⁺ reservoir cells in the naive-like clusters C1, C4, and C8. Univariate analysis relying on CD45RA, CD27, and CCR7 confirmed this finding and further showed a significant enrichment of active vRNA⁺ reservoir cells in T_{CM} and a trend for T_{TM} (Figures 4F, 4G, S3B, and S3C). The paucity of naive active vRNA⁺ reservoir cells is consistent with the significant negative association between the prevalence of naive CD4⁺ T cells and the frequency of active reservoirs (Figure S3D).

Active reservoirs were enriched in clusters C2, C6, and C7 defined by the expression of CCR6 and/or CCR4, suggesting preferential Th17 or Th22 differentiation. C2 and C6 were also enriched in CXCR5 expression, a marker enriched in T follicular helper (Tfh) cells, but this chemokine receptor was not expressed by cells clustering in C7. C7 also included relatively

rare cells with strong features of activation, including higher FI for ICOS, HLA-DR, Ki67, and PD-1 (Figure S3A). Although, we detected frequent active vRNA⁺ reservoir cells in the Th1-like CXCR3-enriched clusters C5 and C3, these subsets were not enriched in infected cells compared with the global CD4⁺ T cell population.

We next analyzed the polarization and integrin and activation marker expression of the active reservoirs through univariate analyses (Figures 4H, 4I, and S3E–S3L). We focused these analyses on CD45RA[−] vRNA⁺ cells to avoid biasing our phenotyping given the near complete absence of vRNA⁺ cells in naive populations. Active vRNA⁺ reservoirs could express any of the four chemokine receptors tested (Figure S3E), with no clear dominance for one over another (Figure S3F). Confirming the previous unsupervised findings, significant enrichments were observed for CCR6⁺ and CCR4⁺ cells, with trends for CXCR5 and CXCR3 (Figures 4H and S3G). CCR6 stood out as the most consistently enriched chemokine receptor among all tested participants (increase in all 16/18 participants). A trend for enrichment of vRNA⁺ events in β 7-integrin⁺ cells was observed, but not in CD103⁺ cells, nor CD32a, another marker previously associated with viral transcription⁴⁹ (Figures S3H–S3J). HLA-DR and Ki67 expression was infrequent in vRNA⁺ cells (2%–15%) (Figures S3K and S3L). ICOS and PD-1 expression was more heterogeneous, with frequencies reaching a much higher level in some participants (2%–43%). Irrespective of their range, all these activation markers except for Ki67, appeared significantly enriched in active vRNA⁺ reservoir cells compared with the global CD4⁺ T cells (Figure 4I).

We next tested whether the magnitude of the inducible reservoir correlated with specific spontaneous vRNA⁺ reservoir clusters (Figure 4J). Several correlations were observed at varying degrees. The connections appeared particularly strong and significant with C3, C6, and C7, which corresponded to the enriched CCR6⁺/CCR4⁺ vRNA⁺ active reservoirs. Because inducible reservoirs could not be reliably phenotyped, we could not relate active reservoirs to inducible reservoir subsets.

These multivariate and univariate analyses provide complementary portraits of peripheral blood active vRNA⁺ cell phenotypes. These cells tend to be memory CD4⁺ T cells, particularly T_{CM}. Compared with other memory CD4⁺ T cells, they are polarized, with a consistent enrichment for CCR6, a marker associated with Th17 and Th22 differentiation, and are more frequently activated than the global CD4⁺ T cell population.

Spontaneously active reservoirs are associated with HIV-specific CD4⁺ and CD8⁺ T cell responses

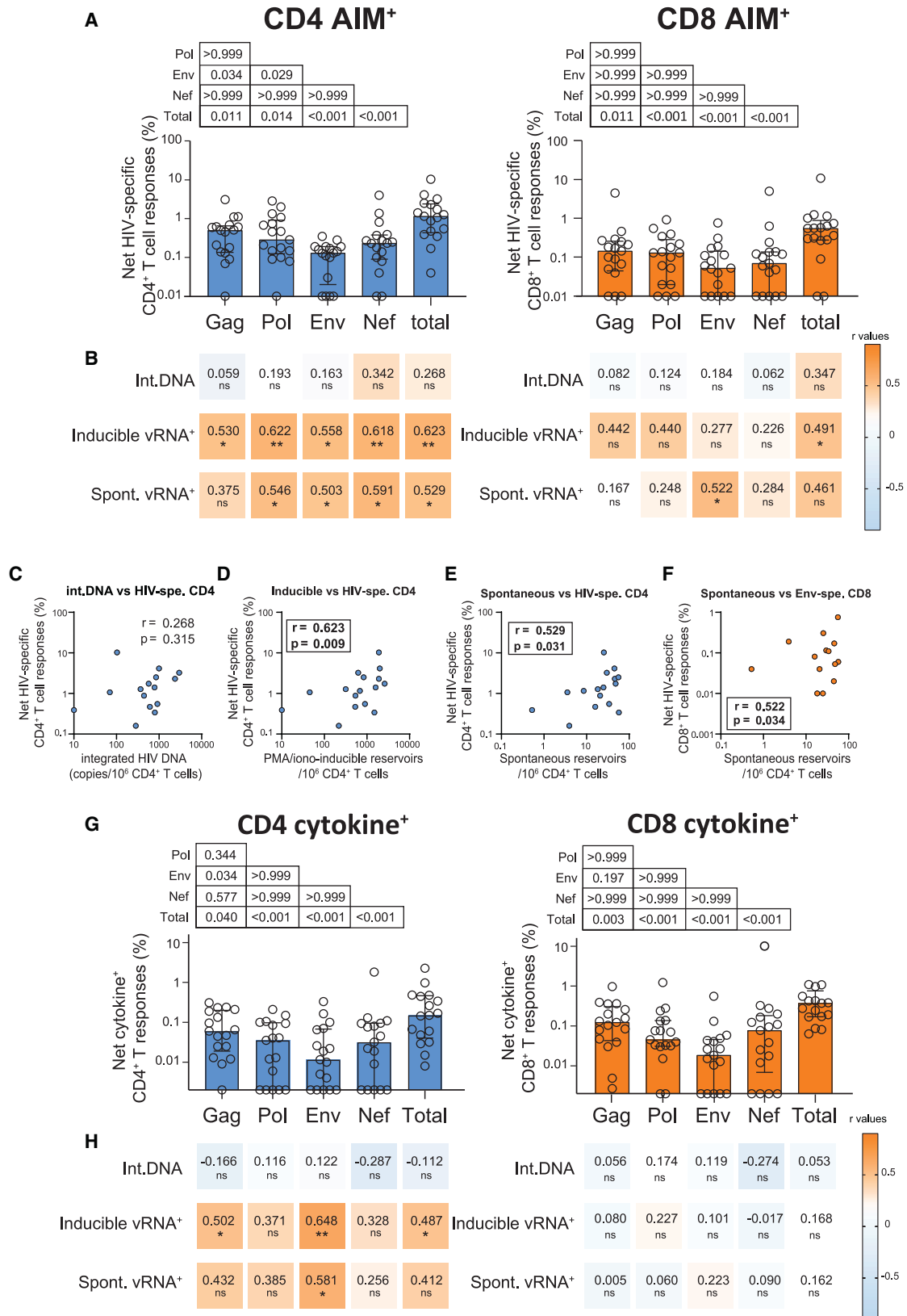
We next tested whether infected cells spontaneously expressing vRNA⁺ could fuel adaptive cellular immunity against HIV during ART. We used a T cell receptor (TCR)-dependent activation-induced marker (AIM) assay that broadly identifies antigen-specific T cells^{29,50,51} (Table S3). We complemented these data with functional profiling by intracellular cytokine staining (ICS) (flow

(F) Donut charts presenting the median proportions of each memory vRNA⁺ subpopulation for spontaneous or PMA/ionomycin-induced reservoirs.

(G–I) Enrichment scores for univariate analysis of (H) memory, (I) polarization, and (J) activation subsets. The enrichment scores were calculated as in (E).

(J) Correlations between PMA/ionomycin- or Panobinostat + ingenol-inducible reservoirs and each active vRNA⁺ cluster. Values and the shade of color indicate r values. p values are shown underneath: *p < 0.05, **p < 0.01, ***p < 0.001.

In (D), (E), and (G)–(I), the histograms indicate the median, and the error bars illustrate the interquartile range and bold values indicate statistical significance.



(legend on next page)

cytometry panels: Table S4). The AIM assay was previously shown to allow a broader capture of antigenic responses than standard ICS, even in the context of CD4⁺ T cell dysfunction.^{29,50}

The AIM assay involved a 15-h incubation of autologous PBMCs with an overlapping peptide pool spanning the coding sequences of either Gag, Pol, Env, or Nef. In CD4⁺ T cells, specificity for these peptides was inferred by the upregulation of CD69, CD40L, 4-1BB, and OX-40 upon stimulation, compared with unstimulated controls, whereas CD69 and 4-1BB co-expression was used for CD8⁺ T cells. We used an AND/OR Boolean combination gating to assess the total frequencies of antigen-specific CD4⁺ and CD8⁺ T cells^{50–52} (Figure S4A). Cells co-expressing at least one pair of AIM were deemed HIV-specific. The significant increases compared with unstimulated conditions confirmed the assay's specificity (Figure S4B).

Effector CD4⁺ and CD8⁺ T cell functions were measured by a 6-h ICS using the same stimulation conditions as for the AIM assays. We focused on interferon-gamma (IFN- γ), interleukin-2 (IL-2), and tumor necrosis factor (TNF) expression. We also defined total cytokine⁺CD4⁺, and cytokine⁺CD8⁺ T cell responses by an OR Boolean gating strategy (Figure S4C). Most participants showed cytokine⁺CD4⁺ and cytokine⁺CD8⁺ T cell responses, although cytokine⁺ CD8⁺ T responses were smaller and more frequently undetectable (Figure S4D).

Gag, Pol, Env, and Nef responses were all readily detectable (Figure 5A). We used the sum of the net responses to each peptide pool to quantify “total” HIV responses. We next correlated total HIV, Gag, Pol, Env, and Nef responses to cells harboring integrated HIV DNA, PMA/ionomycin-inducible, and spontaneously active reservoirs (Figure 5B). There was no significant correlation between AIM⁺ CD4⁺ and CD8⁺ T cell responses and integrated DNA (Figures 5B and 5C). In contrast, inducible reservoirs were strongly associated with total HIV-specific CD4⁺ T cell responses defined by AIM (Figures 5B and 5D). Similar association existed when considering Gag, Pol, Env, and Nef-specific CD4⁺ T cells. A strong correlation was also found between the magnitude of the spontaneous reservoir and total HIV-specific CD4⁺ T cell responses (Figures 5B and 5E). The correlation with Nef was particularly strong ($r = 0.591$), whereas the correlation with Gag ($r = 0.375$) was the weakest. The association between active reservoir cells and total HIV-specific CD8⁺ T cell responses was weaker than with CD4, yet there was a trend. Individual peptide analyses revealed a significant correlation of the active reservoir cells with Env-specific CD8⁺ T cell responses (Figures 5B and 5F, $r = 0.522$). Correlations with Gag, Pol, or Nef-specific CD8⁺ T cell responses were weaker and did not reach significance.

Cytokine⁺ Gag-specific responses were also slightly higher for CD4⁺ and CD8⁺ T cell responses (Figure 5G). The correlation between reservoir metrics and ICS was weaker than with AIM (Figure 5H), possibly due to the lower sensitivity of functional assays. Total HIV-specific CD4⁺ T cells correlated with inducible reservoirs, and a strong trend was observed with active reservoirs. For both inducible and active reservoirs, strong correlations were observed with Env-specific cytokine⁺ CD4⁺ T cells (Figure 5H). The other correlations were weaker and only Gag-specific cytokine⁺ CD4⁺ T cells, for inducible reservoirs, reached significance. No correlation was observed with CD8⁺ T cell effector functions (Figure 5H). These data suggest that active reservoirs and HIV-specific immune responses, particularly Thelper responses, are connected.

A subset of active reservoirs displays stronger links to HIV-specific CD4⁺ and CD8⁺ T cell responses

Next, we performed an unsupervised analysis to characterize HIV-specific CD4⁺ T cells. To account for the inherent phenotypic diversity of circulating CD4⁺ T cells and avoid a-priori-defined marker combinations, we performed an unsupervised analysis of the high-dimensional flow cytometric phenotyping data including total (Gag + Pol + Env + Nef) HIV-specific CD4⁺ T cells. We used chemokine receptors, activation markers and a key immune checkpoint (CXCR5, CXCR3, CCR6, CD38 and HLA-DR, and PD-1). The various clusters were represented using UMAP, and clusters were identified by PhenoGraph. 15 clusters were identified (Figure 6A) based on distinct profiles of relative marker expression (Figures S5A and S5B). Each of these clusters represented 3%–12% of total responses, with the largest C2 and C4 clusters representing no more than 13% of the total population examined (Figure 6B). To simplify the analysis, we grouped these clusters into 6 “superclusters” defined by the expression of chemokine receptors (Figures 6A, 6B, and S5B). The superclusters, ranked by decreasing frequencies, were characterized by the expression of (1) CCR6, (2) none of the tested chemokine receptor, (3) CXCR3, (4) CXCR3 and CCR6, (5) CXCR5, and (6) CXCR5 and CXCR3. Based on previous studies,^{53,54} these superclusters would correspond respectively to (1) T_H17, (2) unpolarized cells, (3) T_H1, (4) non-conventional T_H1 (T_H1*), (5) cTfh, and (6) a T_H1-like subset of cTfh. The frequencies of HIV-specific superclusters in total CD4⁺ T cells showed great variability among participants (Figure S5C), indicating that HIV-specific CD4⁺ T cell responses can adopt very different profiles during ART.

As our results showed relationships between active reservoirs and immune responses, we next examined how associations

Figure 5. Associations between spontaneously active reservoirs and HIV-specific CD4⁺ and CD8⁺ T cell responses

- (A) Net magnitude of HIV-specific CD4⁺ and CD8⁺ T cells by AIM assay.
 (B) Heatmap reporting the associations between AIM⁺ CD4⁺ and CD8⁺ T responses and integrated DNA, inducible and spontaneously active reservoirs.
 (C–E) Correlations between net AIM⁺ CD4⁺ responses and (C) integrated DNA, (D) inducible reservoirs, and (E) spontaneous reservoirs.
 (F) Correlation between net AIM⁺ CD8⁺ T cell responses and spontaneous reservoirs.
 (G) Net magnitude of HIV-specific CD4⁺ and CD8⁺ T cells defined by the ICS.
 (H) Heatmap reporting the associations between cytokine⁺ CD4⁺ and cytokine⁺ CD8⁺ T responses and integrated DNA, inducible and spontaneously active reservoirs.

In (A), (B), (G), and (H), peptide pools used to stimulate PBMCs are indicated. “HIV” responses were inferred by the sum of Gag, Pol, Env, and Nef net responses. In (A) and (G), net magnitudes after background subtraction are shown. The bars indicate the median, and the error bars illustrate the interquartile range. The results from a Friedman test are shown above. In (B) and (H), r and p (Spearman) values are shown. $p < 0.05$, $**p < 0.01$, $***p < 0.001$. $n = 16$ (1 participant had <5 vRNA⁺ cells, therefore could not be phenotyped).

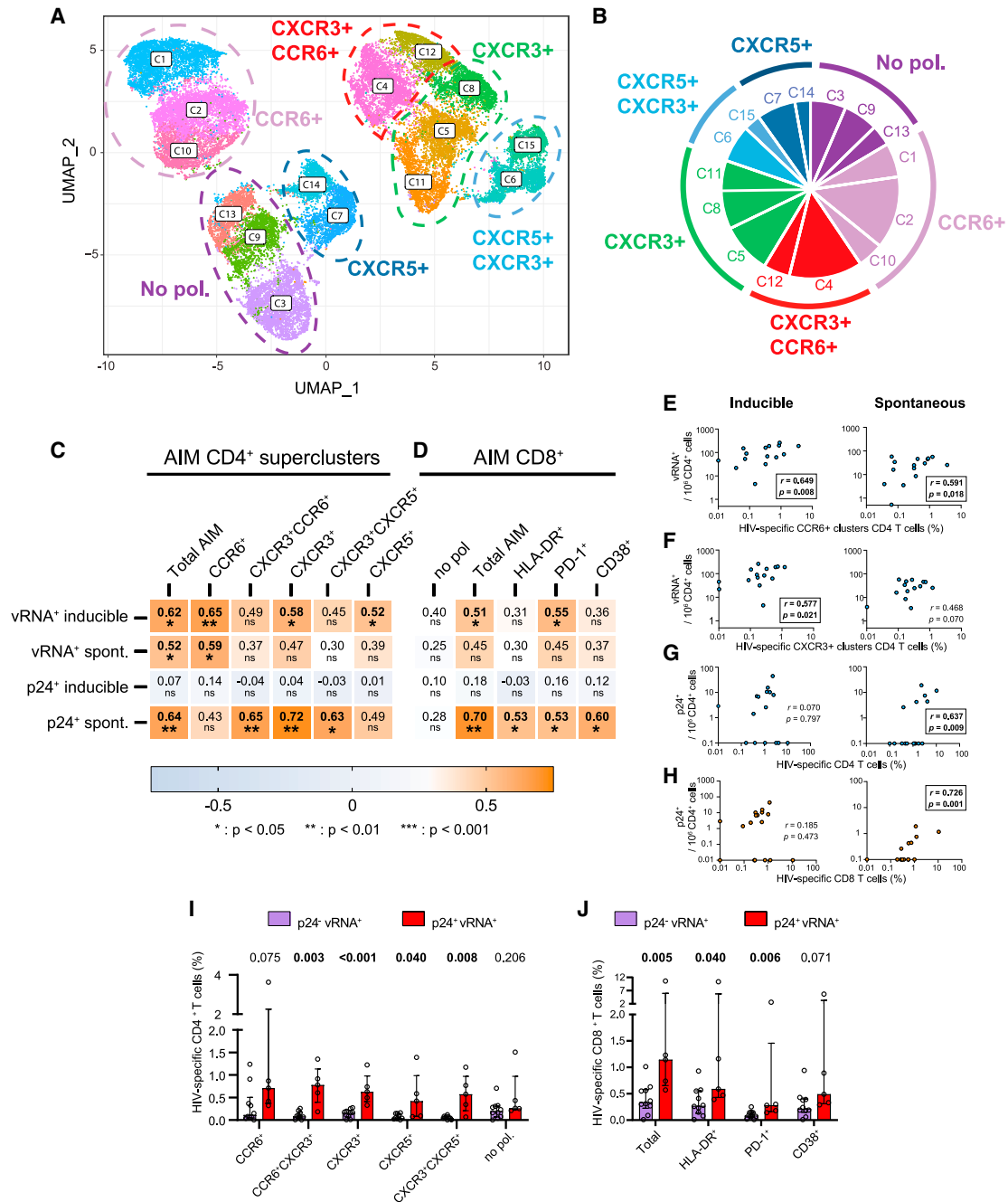


Figure 6. A subset of active reservoirs display strong links to HIV-specific CD4⁺ and CD8⁺ T cell responses

(A) Global uniform manifold approximation and projection (UMAP) for dimension reduction map of HIV-specific AIM⁺ CD4⁺ T cells. 15 clusters were identified and regrouped in 6 superclusters.

(B) Median proportions of each cluster, regrouped by superclusters.

(C and D) Heatmap showing correlations between (C) vRNA⁺ cluster frequencies and net magnitudes of AIM⁺ CD4⁺, regrouped by superclusters, or (D) vRNA⁺ cluster frequencies and net magnitudes of AIM⁺ CD8⁺ T cells. p values from Spearman test are shown, with significance underneath. *p < 0.05, **p < 0.01, ***p < 0.001.

(E and F) Correlations between the inducible or spontaneous vRNA⁺ reservoir and the magnitude of cells in (E) AIM⁺ HIV-specific CCR6⁺ CD4⁺ T cell supercluster and (F) AIM⁺ HIV-specific CXCR3⁺ CD4⁺ T cell supercluster.

(G and H) Correlations between the inducible or spontaneous p24⁺ reservoir and the magnitude of cells in (G) total AIM⁺ HIV-specific CD4⁺ and (H) total AIM⁺ HIV-specific CD8⁺ T cells. Spearman tests were performed. r and p values are shown.

(I and J) Histogram comparing median HIV-specific AIM⁺ (I) CD4⁺ and (J) CD8⁺ T cell responses in people where p24⁺ cells were detectable in peripheral blood (n = 5) or were not (n = 11). Mann-Whitney tests are shown above. Error bars indicate the interquartile range. n = 16 (1 participant had <5 vRNA⁺ cells, therefore could not be phenotyped).

varied between types of viral reservoirs and subpopulations of HIV-specific AIM⁺ CD4⁺ and CD8⁺ T cells. Our first layer of analysis focused on total HIV-specific CD4⁺ T cell superclusters (Figure 6C). We found a strong correlation between the magnitude of both inducible or spontaneous vRNA⁺ cells and total AIM⁺ CD4⁺ T cell responses (Figure 6C). For the spontaneous reservoirs, correlations with CCR6⁺ AIM⁺ CD4⁺ T cell responses was particularly strong (Figures 6C and 6E), and showed a trend with CXCR3⁺ AIM⁺ CD4⁺ T cell responses (Figures 6C and 6F). Inducible vRNA⁺ cells showed significant correlations with total and PD1⁺ AIM⁺ CD8⁺ T cell responses (Figure 6D). The correlations between spontaneous vRNA⁺ cells and total and PD1⁺ AIM⁺ CD8⁺ T cell responses showed trends. Associations with HLA-DR⁺ and CD38⁺ responses were weaker.

We observed a significant correlation between active p24⁺ reservoirs and total AIM⁺ specific CD4⁺ T cells (Figures 6C and 6G). The *r* value (*r* = 0.720) was particularly strong for the CXCR3⁺ supercluster (Figure 6C). We also noted strong correlations of total and activated AIM⁺ specific CD8 T cells with active p24⁺ reservoirs (Figures 6D and 6H). Correlations were lost with PMA/ionomycin-induced p24⁺ reservoirs, indicating that, critically, only spontaneously p24-expressing cells can shape HIV-specific CD4⁺ and CD8⁺ T cell responses. We divided our cohort based on whether p24⁺ could or could not be detected among vRNA⁺ cells (Figure 2F). HIV-specific CD4⁺ and CD8⁺ T cell responses were significantly higher in the p24⁺ group (Figures 6I and 6J). There were marked differences between the two groups for CXCR3⁺ and CXCR3⁺ CXCR5⁺ superclusters, suggesting that protein expression is a prerequisite for their maintenance.

Together, these results demonstrate important relationships between spontaneous vRNA⁺ and—especially—p24-expressing viral reservoirs and magnitude and function of HIV-specific CD4⁺ and CD8⁺ T cell responses.

DISCUSSION

In this study, we characterized HIV reservoirs spontaneously expressing viral transcripts, as detected at the single-cell level by RNAflow-FISH. We identified these active reservoir cells in most PWH investigated, at a frequency only 3-fold lower than the PMA/ionomycin-inducible reservoirs. We phenotyped these active reservoirs without the confounding impact of LRAs. Integrated analyses demonstrated the heterogeneous nature of active vRNA⁺ reservoirs. Certain features were enriched, such as high expression of CCR6, a marker of Th17 and Th22 cells. We found associations between active viral reservoirs and HIV-specific CD4⁺ and CD8⁺ T cell responses during suppressive ART. CCR6⁺ HIV-specific CD4⁺ T cells seemed particularly connected to various active reservoirs. HIV-specific CD4⁺ and CD8⁺ T cell responses were higher in the few participants in which active p24⁺ reservoir cells could be detected, suggesting that maintaining those immune responses requires spontaneous viral translation.

We and others previously showed how the RNAflow-FISH assay could identify reactivated viral reservoirs at the single-cell level.^{8,9,55} By adapting a multigene HIV-specific probe set design, we detected viral reservoirs with great sensitivity and resolution without *ex vivo* latency reversal. Spontaneous and inducible vRNA⁺ reservoirs correlated. One possible explanation

for this relationship is that they represent two facets of the same cell: latency reversal could exacerbate pre-existing, very low-yield transcriptional activity possibly missed by our experimental technique. These cells may be poised for higher transcriptional activity upon induction, as suggested by the higher median fluorescence intensity (MFI) for the vRNA signal in induced vs spontaneously active cells. The low transcriptional activity may be due to (1) suboptimal Tat-mediated transactivation during latency,⁵⁶ (2) the shortness of the abortive transcripts, consistent with data previously obtained by digital-droplet PCR,^{10,41} that may make them less sensitive to detection by a branched DNA amplification technique, and (3) the requirement for staining with two HIV RNA probe sets can reduce sensitivity of detection. Alternatively, a portion of the PMA/ionomycin-inducible reservoirs may have been in a deeper state of latency and fully silent prior to stimulation,^{57–59} therefore only revealed after pharmacological reactivation. Spontaneous viral gene expression was also characterized by a shorter transcription and rare translation of Gag. These observations are consistent with previous reports and suggest transcriptional¹⁰ and post-transcription blocks⁶⁰ to viral gene expression.

Another notable finding of our study is that active reservoirs are not confined to any specific CD4⁺ T subset. This finding is consistent with recent reports correlating viral transcriptomic and genomic properties.^{60,61} All CD4⁺ clusters we analyzed were populated to some degree with vRNA⁺ reservoirs. Yet, compared with total peripheral CD4⁺ T cells, active reservoir cells profiles were (1) rarely naive and mostly T_{CM}, (2) enriched in CCR6, suggesting a preferential Th17 and Th22 polarization, (3) enriched in activation and exhaustion markers such as HLA-DR, ICOS, and PD-1, and (4) enriched with cell proliferation marker Ki67. Although modest, enrichment in activation/exhaustion and proliferation markers is consistent with homeostatic^{62–64} and antigen-driven proliferation reported during ART.^{34,65} Although we observed some enrichment of activation markers in active reservoirs, the vast majority of spontaneous reservoir cells were still found in cells that did not express activation markers, indicating that T cell activation is not a prerequisite for spontaneous viral gene expression. The enrichment of HIV-infected cells we have observed in T_{CM}, CCR6, and to a lesser extent, CXCR5 and CXCR3 are consistent with previous reports using univariate analyses.^{62,66–71} These enrichments may reflect preferential replication of HIV-1 in specific anatomic compartments before ART initiation, such as the intestinal mucosa (hence the enrichment in the gut homing and Th17 marker CCR6)^{8,72,73} and germinal centers of lymph nodes (hence the enrichment in the Tfh marker CXCR5).^{8,72,73} Some tissues and microenvironments (e.g., gastrointestinal tract) may also be more permissive to viral transcription,^{74,75} and this would be mirrored in the circulation when these cells egress from tissues into the blood. We cannot exclude that residual replication occurs in tissues where penetration of antivirals may be suboptimal. However, to date, no direct evidence has shown that ongoing viral replication contributes to viral reservoir persistence in PWH receiving suppressive ART.^{33,35,36}

An association was previously reported between cytotoxic Nef-specific CD8⁺ T cell responses and HIV DNA and RNA.⁷⁶ Using single-cell approaches, we now find multiple strong positive correlations between active reservoirs and the magnitude of Pol,

Env, Nef, and to a lesser extent, Gag-specific CD4⁺ and CD8⁺ T cell responses, indicating a broader relationship than initially anticipated. The correlations were always stronger with HIV RNA than with HIV DNA, suggesting that some gene expression is necessary to reveal these relationships. Detailed analyses showed that the strength of these correlations varied among the pairs of viral and immune clusters assessed, suggesting that viral reservoirs do not all influence anti-HIV immune responses equally. HIV-specific CCR6⁺ CD4⁺ clusters were particularly well correlated with active reservoir cells. While this correlation suggests tissue-specific interface between active reservoirs and HIV-specific T cells, putatively the gut, further investigations will be necessary to deeply decipher connections between reservoirs and HIV-specific immune responses.

The positivity of the relationship suggests that spontaneous reservoirs are sustaining HIV-specific CD4⁺ and CD8⁺ T cells rather than HIV-specific cells controlling the reservoirs. In this later case, a negative association would have been expected. However, spontaneously active reservoirs that still persist after >3 post-ART initiation and reservoir selection by the immune system are likely inherently more resistant to cell death. Consistent with this, recent studies showed that persistent reservoirs adopt a pro-survival gene expression profile.^{60,77,78} How viral transcription may drive immune responses remains a key question. The magnitude of HIV-specific CD4⁺ and CD8⁺ T cell responses were lower in participants with no spontaneous p24-expressing active reservoir. In contrast, these responses were robust in participants in which p24-expressing vRNA⁺ reservoir cells could be detected. These findings suggest that viral protein expression, although rare, is the driving force keeping HIV reservoirs and HIV-specific immune responses closely related. It will be important to determine whether spontaneous expression of Gag and other HIV proteins is more frequent in specific tissues, possibly the gut due to proinflammatory microenvironment more favorable for provirus activation or in anatomic compartments harboring a weaker immune surveillance.⁷⁹ Alternatively, sporadic Gag expression in peripheral blood, perhaps during transient challenges such as acute illnesses could possibly contribute to the antigen-stimulated maintenance of HIV-specific immunity. If this is the case, active vRNA⁺ reservoir cells in the circulation may mirror tissue reservoir cells that are prone to produce proteins and subsequently cognate peptides presented by major histocompatibility complex (MHC) molecules to T cells.

Inducible proviruses can bear not only minor,^{9,17} but extensive defects predicted to prevent viral replication. We showed here that spontaneously active reservoirs are mostly defective as well. Yet, reservoirs expressing transcripts from these defective proviruses may still allow some translation,^{37,38,80} depending on where the defect is located. Our work supports that such defective proviruses can also maintain HIV-specific CD4⁺ and CD8⁺ T cell responses in a chronic state of expansion, activation, and exhaustion during ART.

Our study has some limitations. Only Caucasian males were included mostly due to the epidemiology of the PWH population in Montreal and, to some extent, the more frequent difficulties for peripheral vein access to perform leukaphereses in females. It will be important to conduct such studies in women and in other ethnicities, as immune responses may vary with sex and genetic background. ART was initiated in most participant's years after

HIV acquisition; investigations of PWH who initiated therapy early would provide valuable complementary information. While the assay used allows high-parameter profiling of active reservoir cells, our conservative detection limit (about 5 vRNA copies/cell)^{8,43} missed the lowest levels of gene transcription. Other approaches indeed indicated even higher magnitudes of spontaneous reservoirs.⁸¹ Studies of gut and other lymphoid tissues will be important to gain a deeper understanding of the immunovirological dynamics involved. The relatively small size of the cohort studied did not allow us to reliably rank the strength of the associations between active reservoir clusters and HIV-specific T cell superclusters.

Finally, our study may have notable implications for HIV cure strategies. Approaches considered include Env-specific broadly neutralizing antibodies. The fraction of active reservoirs that are competent for Env expression will impact the potential effectiveness of such therapies to eliminate these cells. While the replication-competent HIV reservoir is the primary target of HIV cure, our data highlight the pathophysiologic relevance of other fractions of the HIV reservoirs, likely contributing to the deleterious effect of immune activation. Research efforts should also consider the putatively negative impact of spontaneously active reservoirs in the design of interventions aiming at clinical benefit for PWH on suppressive ART.

STAR★METHODS

Detailed methods are provided in the online version of this paper and include the following:

- KEY RESOURCES TABLE
- RESOURCE AVAILABILITY
 - Lead contact
 - Materials availability
 - Data and code availability
- EXPERIMENTAL MODEL AND SUBJECT DETAILS
 - Ethics Statement
 - Participants and Samples
- METHOD DETAILS
 - Total and integrated DNA measures
 - CD4⁺ T cell preparation for HIV reservoir profiling
 - HIV-1 RNAflow-FISH assay
 - Limiting Dilution Assay
 - Microscopy
 - Single-cell near full-length PCR
 - Activation-induced marker (AIM) assay
 - Intracellular Cytokine Staining (ICS)
- QUANTIFICATION AND STATISTICAL ANALYSIS
 - Statistical analysis
 - Software scripts and visualization

SUPPLEMENTAL INFORMATION

Supplemental information can be found online at <https://doi.org/10.1016/j.chom.2023.08.006>.

ACKNOWLEDGMENTS

We thank Josée Girouard, Angie Massicotte (CUSM), and all study participants for their invaluable role in this project; Dr. Dominique Gauchat, Dr. Gaël

Dulude, Philippe St-Onge, and the CRCHUM Flow Cytometry Platform; Dr. Olfa Debbeche and the CRCHUM BSL3 platform; and Aurélie Cleret-Buhot and the Microscopy platform. The following reagents were obtained through the NIH HIV Reagent Program, Division of AIDS, NIAID: Maraviroc (ARP-11580), Raltegravir (ARP-11680), Tenofovir (ARP-10199), and Emtricitabine (ARP-10071). Funding: this study was supported by the Canadian Institutes for Health Research (CIHR grant #152977 to D.E.K.), the US National Institutes of Health (R01AI14341 to J.D.E., N.C., and D.E.K.), and the Réseau Fonds de la recherche Québec-Santé (FRQS) SIDA & Maladies infectieuses and thérapies cellulaires. D.E.K. is an FRQS Merit Research Scholar. N.C. is an FRQS Research Scholar awardee. G.S. is supported by an FRQS doctorate fellowship and by a scholarship from the Department of Microbiology, Infectious Disease, and Immunology of the University of Montreal. J.D.E. is supported by the Oregon National Primate Research Center grant award P51OD011092. The Symphony flow cytometer was funded by a John R. Evans Leaders Fund Leader Fund from the Canada Foundation for Innovation (fund #37521 to D.E.K.) and the Fondation Sclérodémie Québec.

AUTHOR CONTRIBUTIONS

Conceptualization and supervision, M.D. and D.E.K.; methodology, M.D., G.S., and N.B.; software, O.T.; investigation and validation, G.-G.D., M.D., N.B., G.S., M.N., and A. Pagliuzza; formal analysis, M.D., O.T., C.D., C.R., and R.F. J.-P.R. ensured recruitment and clinical assessments. Data curation, C.R. and M.D.; interpretation, M.D., O.T., A. Pagliuzza, R.F., J.D.E., N.C., and D.E.K. J.D.E. and A. Prat provided intellectual input. Writing – original draft, M.D. and D.E.K.; review & editing, all co-authors; visualization, M.D., C.D., and O.T.; project administration, M.D.; funding acquisition, D.E.K., N.C., and J.D.E.

DECLARATION OF INTERESTS

The authors declare no competing interests.

Received: January 24, 2023

Revised: June 1, 2023

Accepted: August 11, 2023

Published: September 13, 2023

REFERENCES

- Davey, R.T., Jr., Bhat, N., Yoder, C., Chun, T.W., Metcalf, J.A., Dewar, R., Natarajan, V., Lempicki, R.A., Adelsberger, J.W., Miller, K.D., et al. (1999). HIV-1 and T cell dynamics after interruption of highly active antiretroviral therapy (HAART) in patients with a history of sustained viral suppression. *Proc. Natl. Acad. Sci. USA* *96*, 15109–15114. <https://doi.org/10.1073/pnas.96.26.15109>.
- Baxter, A.E., O'Doherty, U., and Kaufmann, D.E. (2018). Beyond the replication-competent HIV reservoir: transcription and translation-competent reservoirs. *Retrovirology* *15*, 18. <https://doi.org/10.1186/s12977-018-0397-2>.
- Gaebler, C., Lorenzi, J.C.C., Oliveira, T.Y., Nogueira, L., Ramos, V., Lu, C.-L., Pai, J.A., Mendoza, P., Jankovic, M., Caskey, M., and Nussenzweig, M.C. (2019). Combination of quadruplex qPCR and next-generation sequencing for qualitative and quantitative analysis of the HIV-1 latent reservoir. *J. Exp. Med.* *216*, 2253–2264. <https://doi.org/10.1084/jem.20190896>.
- Bruner, K.M., Wang, Z., Simonetti, F.R., Bender, A.M., Kwon, K.J., SenGupta, S., Fray, E.J., Beg, S.A., Antar, A.A.R., Jenike, K.M., et al. (2019). A quantitative approach for measuring the reservoir of latent HIV-1 proviruses. *Nature* *566*, 120–125. <https://doi.org/10.1038/s41586-019-0898-8>.
- Procopio, F.A., Fromentin, R., Kulpa, D.A., Brehm, J.H., Bebin, A.G., Strain, M.C., Richman, D.D., O'Doherty, U., Palmer, S., Hecht, F.M., et al. (2015). A novel assay to measure the magnitude of the inducible viral reservoir in HIV-infected individuals. *EBioMedicine* *2*, 874–883. <https://doi.org/10.1016/j.ebiom.2015.06.019>.
- Pasternak, A.O., and Berkhout, B. (2018). What do we measure when we measure cell-associated HIV RNA. *Retrovirology* *15*, 13. <https://doi.org/10.1186/s12977-018-0397-2>.
- Pardons, M., Baxter, A.E., Massanella, M., Pagliuzza, A., Fromentin, R., Dufour, C., Leyre, L., Routy, J.P., Kaufmann, D.E., and Chomont, N. (2019). Single-cell characterization and quantification of translation-competent viral reservoirs in treated and untreated HIV infection. *PLoS Pathog.* *15*, e1007619. <https://doi.org/10.1371/journal.ppat.1007619>.
- Baxter, A.E., Niessl, J., Fromentin, R., Richard, J., Porichis, F., Charlebois, R., Massanella, M., Brassard, N., Alshafiq, N., Delgado, G.-G., et al. (2016). Single-cell characterization of viral translation-competent reservoirs in HIV-infected individuals. *Cell Host Microbe* *20*, 368–380. <https://doi.org/10.1016/j.chom.2016.07.015>.
- Sannier, G., Dubé, M., Dufour, C., Richard, C., Brassard, N., Delgado, G.G., Pagliuzza, A., Baxter, A.E., Niessl, J., Brunet-Ratnasingham, E., et al. (2021). Combined single-cell transcriptional, translational, and genomic profiling reveals HIV-1 reservoir diversity. *Cell Rep.* *36*, 109643. <https://doi.org/10.1016/j.celrep.2021.109643>.
- Yukl, S.A., Kaiser, P., Kim, P., Telwatte, S., Joshi, S.K., Vu, M., Lampiris, H., and Wong, J.K. (2018). HIV latency in isolated patient CD4⁺ T cells may be due to blocks in HIV transcriptional elongation, completion, and splicing. *Sci. Transl. Med.* *10*, eaap9927. <https://doi.org/10.1126/scitranslmed.aap9927>.
- Mohammadi, P., di Iulio, J., Muñoz, M., Martinez, R., Bartha, I., Cavassini, M., Thorball, C., Fellay, J., Beerenwinkel, N., Ciuffi, A., and Telenti, A. (2014). Dynamics of HIV latency and reactivation in a primary CD4⁺ T cell model. *PLoS Pathog.* *10*, e1004156. <https://doi.org/10.1371/journal.ppat.1004156>.
- Dornadula, G., Zhang, H., VanUitert, B., Stern, J., Livornese, L., Jr., Ingberman, M.J., Witek, J., Kedanis, R.J., Natkin, J., DeSimone, J., and Pomerantz, R.J. (1999). Residual HIV-1 RNA in blood plasma of patients taking suppressive highly active antiretroviral therapy. *JAMA* *282*, 1627–1632. <https://doi.org/10.1001/jama.282.17.1627>.
- Günthard, H.F., Havlir, D.V., Fiscus, S., Zhang, Z.-Q., Eron, J., Mellors, J., Gulick, R., Frost, S.D., Brown, A.J., Schleif, W., et al. (2001). Residual human immunodeficiency virus (HIV) type 1 RNA and DNA in lymph nodes and HIV RNA in genital secretions and in cerebrospinal fluid after suppression of viremia for 2 years. *J. Infect. Dis.* *183*, 1318–1327. <https://doi.org/10.1086/319864>.
- Halvas, E.K., Joseph, K.W., Brandt, L.D., Guo, S., Sobolewski, M.D., Jacobs, J.L., Tumiottio, C., Bui, J.K., Cyktor, J.C., Keele, B.F., et al. (2020). HIV-1 viremia not suppressible by antiretroviral therapy can originate from large T cell clones producing infectious virus. *J. Clin. Invest.* *130*, 5847–5857. <https://doi.org/10.1172/JCI138099>.
- Ishizaka, A., Sato, H., Nakamura, H., Koga, M., Kikuchi, T., Hosoya, N., Koibuchi, T., Nomoto, A., Kawana-Tachikawa, A., and Mizutani, T. (2016). Short intracellular HIV-1 transcripts as biomarkers of residual immune activation in patients on antiretroviral therapy. *J. Virol.* *90*, 5665–5676. <https://doi.org/10.1128/JVI.03158-15>.
- Fischer, M., Günthard, H.F., Opravil, M., Joos, B., Huber, W., Bisset, L.R., Ott, P., Böni, J., Weber, R., and Cone, R.W. (2000). Residual HIV-RNA levels persist for up to 2.5 years in peripheral blood mononuclear cells of patients on potent antiretroviral therapy. *AIDS Res. Hum. Retroviruses* *16*, 1135–1140. <https://doi.org/10.1089/088922200414974>.
- White, J.A., Wu, F., Yasin, S., Moskovljevic, M., Varriale, J., Dragoni, F., Camilo-Contreras, A., Duan, J., Zheng, M.Y., Tadzong, N.F., et al. (2023). Clonally expanded HIV-1 proviruses with 5'-Leader defects can give rise to nonsuppressible residual viremia. *J. Clin. Invest.* *133*, e165245. <https://doi.org/10.1172/JCI165245>.
- Ferdin, J., Goričar, K., Dolžan, V., Plemenitas, A., Martin, J.N., Peterlin, B.M., Deeks, S.G., and Lenassi, M. (2018). Viral protein Nef is detected in plasma of half of HIV-infected adults with undetectable plasma HIV RNA. *PLoS ONE* *13*, e0191613. <https://doi.org/10.1371/journal.pone.0191613>.

19. Passaes, C., Delagrèverie, H.M., Avettand-Fenoel, V., David, A., Monceaux, V., Essat, A., Müller-Trutwin, M., Duffy, D., De Castro, N., Wittkop, L., et al. (2021). Ultrasensitive detection of p24 in plasma samples from people with primary and chronic HIV-1 infection. *J. Virol.* *95*, e0001621. <https://doi.org/10.1128/JVI.00016-21>.
20. Wu, G., Zuck, P., Goh, S.L., Milush, J.M., Vohra, P., Wong, J.K., Somsouk, M., Yuki, S.A., Shacklett, B.L., Chomont, N., et al. (2021). Gag p24 is a marker of human immunodeficiency virus expression in tissues and correlates with immune response. *J. Infect. Dis.* *224*, 1593–1598. <https://doi.org/10.1093/infdis/jiab121>.
21. Cartwright, E.K., Spicer, L., Smith, S.A., Lee, D., Fast, R., Paganini, S., Lawson, B.O., Nega, M., Easley, K., Schmitz, J.E., et al. (2016). CD8(+) lymphocytes are required for maintaining viral suppression in SIV-infected macaques treated with short-term antiretroviral therapy. *Immunity* *45*, 656–668. <https://doi.org/10.1016/j.immuni.2016.08.018>.
22. Chevalier, M.F., Jülg, B., Pyo, A., Flanders, M., Ransinghe, S., Soghoian, D.Z., Kwon, D.S., Rychert, J., Lian, J., Muller, M.I., et al. (2011). HIV-1-specific interleukin-21+ CD4+ T cell responses contribute to durable viral control through the modulation of HIV-specific CD8+ T cell function. *J. Virol.* *85*, 733–741. <https://doi.org/10.1128/JVI.02030-10>.
23. Gray, G.E., Huang, Y., Grunenberg, N., Laher, F., Roux, S., Andersen-Nissen, E., De Rosa, S.C., Flach, B., Randhawa, A.K., Jensen, R., et al. (2019). Immune correlates of the Thai RV144 HIV vaccine regimen in South Africa. *Sci. Transl. Med.* *11*, eaax1880. <https://doi.org/10.1126/scitranslmed.aax1880>.
24. Tebas, P., Jadlowsky, J.K., Shaw, P.A., Tian, L., Esparza, E., Brennan, A.L., Kim, S., Naing, S.Y., Richardson, M.W., Vogel, A.N., et al. (2021). CCR5-edited CD4+ T cells augment HIV-specific immunity to enable post-rebound control of HIV replication. *J. Clin. Invest.* *131*, e144486. <https://doi.org/10.1172/JCI144486>.
25. Tuyishime, S., Haut, L.H., Kurupati, R.K., Billingsley, J.M., Carnathan, D., Gangahara, S., Styles, T.M., Xiang, Z., Li, Y., Zopfs, M., et al. (2018). Correlates of protection against SIV_{mac251} infection in rhesus macaques immunized with chimpanzee-derived adenovirus vectors. *EBioMedicine* *31*, 25–35. <https://doi.org/10.1016/j.ebiom.2018.02.025>.
26. International HIV Controllers Study, Pereyra, F., Jia, X., McLaren, P.J., Telenti, A., de Bakker, P.I., Walker, B.D., Ripke, S., Brumme, C.J., Pulit, S.L., et al. (2010). The major genetic determinants of HIV-1 control affect HLA class I peptide presentation. *Science* *330*, 1551–1557. <https://doi.org/10.1126/science.1195271>.
27. Moysi, E., Petrovas, C., and Koup, R.A. (2018). The role of follicular helper CD4 T cells in the development of HIV-1 specific broadly neutralizing antibody responses. *Retrovirology* *15*, 54. <https://doi.org/10.1186/s12977-018-0437-y>.
28. Trautmann, L. (2016). Kill: boosting HIV-specific immune responses. *Curr. Opin. HIV AIDS* *11*, 409–416. <https://doi.org/10.1097/COH.0000000000000286>.
29. Niessl, J., Baxter, A.E., Morou, A., Brunet-Ratnasingham, E., Sannier, G., Gendron-Lepage, G., Richard, J., Delgado, G.-G., Brassard, N., Turcotte, I., et al. (2020). Persistent expansion and Th1-like skewing of HIV-specific circulating T follicular helper cells during antiretroviral therapy. *EBioMedicine* *54*, 102727. <https://doi.org/10.1016/j.ebiom.2020.102727>.
30. Reiss, S., Baxter, A.E., Cirelli, K.M., Dan, J.M., Morou, A., Daigneault, A., Brassard, N., Silvestri, G., Routy, J.P., Havenar-Daughton, C., et al. (2017). Comparative analysis of activation induced marker (AIM) assays for sensitive identification of antigen-specific CD4 T cells. *PLoS ONE* *12*, e0186998. <https://doi.org/10.1371/journal.pone.0186998>.
31. Warren, J.A., Zhou, S., Xu, Y., Moeser, M.J., MacMillan, D.R., Council, O., Kirchherr, J., Sung, J.M., Roan, N.R., Adimora, A.A., et al. (2020). The HIV-1 latent reservoir is largely sensitive to circulating T cells. *eLife* *9*, e57246. <https://doi.org/10.7554/eLife.57246>.
32. Thomas, A.S., Jones, K.L., Gandhi, R.T., McMahon, D.K., Cyktor, J.C., Chan, D., Huang, S.-H., Truong, R., Bosque, A., Macedo, A.B., et al. (2017). T-cell responses targeting HIV Nef uniquely correlate with infected cell frequencies after long-term antiretroviral therapy. *PLoS Pathog.* *13*, e1006629. <https://doi.org/10.1371/journal.ppat.1006629>.
33. Mok, H.P., Norton, N.J., Hirst, J.C., Fun, A., Bandara, M., Wills, M.R., and Lever, A.M.L. (2018). No evidence of ongoing evolution in replication competent latent HIV-1 in a patient followed up for two years. *Sci. Rep.* *8*, 2639. <https://doi.org/10.1038/s41598-018-20682-w>.
34. Simonetti, F.R., Sobolewski, M.D., Fyne, E., Shao, W., Spindler, J., Hattori, J., Anderson, E.M., Watters, S.A., Hill, S., Wu, X., et al. (2016). Clonally expanded CD4+ T cells can produce infectious HIV-1 in vivo. *Proc. Natl. Acad. Sci. USA* *113*, 1883–1888. <https://doi.org/10.1073/pnas.1522675113>.
35. Van Zyl, G.U., Katusiime, M.G., Wiegand, A., McManus, W.R., Bale, M.J., Halvas, E.K., Luke, B., Boltz, V.F., Spindler, J., Laughton, B., et al. (2017). No evidence of HIV replication in children on antiretroviral therapy. *J. Clin. Invest.* *127*, 3827–3834. <https://doi.org/10.1172/JCI94582>.
36. Vancollie, L., Hebberecht, L., Dauwe, K., Demecheleer, E., Dinakis, S., Vaneechoutte, D., Mortier, V., and Verhofstede, C. (2017). Longitudinal sequencing of HIV-1 infected patients with low-level viremia for years while on ART shows no indications for genetic evolution of the virus. *Virology* *510*, 185–193. <https://doi.org/10.1016/j.virol.2017.07.010>.
37. Imamichi, H., Smith, M., Adelsberger, J.W., Izumi, T., Scrimieri, F., Sherman, B.T., Rehm, C.A., Imamichi, T., Pau, A., Catalfamo, M., et al. (2020). Defective HIV-1 proviruses produce viral proteins. *Proc. Natl. Acad. Sci. USA* *117*, 3704–3710. <https://doi.org/10.1073/pnas.1917876117>.
38. Pollack, R.A., Jones, R.B., Perteau, M., Bruner, K.M., Martin, A.R., Thomas, A.S., Capoferri, A.A., Beg, S.A., Huang, S.-H., Karandish, S., et al. (2017). Defective HIV-1 proviruses are expressed and can be recognized by cytotoxic T lymphocytes, which shape the proviral landscape. *Cell Host Microbe* *21*, 494–506.e4. <https://doi.org/10.1016/j.chom.2017.03.008>.
39. Simonetti, F.R., Zhang, H., Soroosh, G.P., Duan, J., Rhodehouse, K., Hill, A.L., Beg, S.A., McCormick, K., Raymond, H.E., Nobles, C.L., et al. (2021). Antigen-driven clonal selection shapes the persistence of HIV-1-infected CD4+ T cells in vivo. *J. Clin. Invest.* *131*, e145254. <https://doi.org/10.1172/JCI145254>.
40. Wiegand, A., Spindler, J., Hong, F.F., Shao, W., Cyktor, J.C., Cillo, A.R., Halvas, E.K., Coffin, J.M., Mellors, J.W., and Kearney, M.F. (2017). Single-cell analysis of HIV-1 transcriptional activity reveals expression of proviruses in expanded clones during ART. *Proc. Natl. Acad. Sci. USA* *114*, E3659–E3668. <https://doi.org/10.1073/pnas.1617961114>.
41. Moron-Lopez, S., Xie, G., Kim, P., Siegel, D.A., Lee, S., Wong, J.K., Price, J.C., Elnachef, N., Greenblatt, R.M., Tien, P.C., et al. (2021). Tissue-specific differences in HIV DNA levels and mechanisms that govern HIV transcription in blood, gut, genital tract and liver in ART-treated women. *J. Int. AIDS Soc.* *24*, e25738. <https://doi.org/10.1002/jia2.25738>.
42. Karn, J., and Stoltzfus, C.M. (2012). Transcriptional and posttranscriptional regulation of HIV-1 gene expression. *Cold Spring Harb. Perspect. Med.* *2*, a006916. <https://doi.org/10.1101/cshperspect.a006916>.
43. Porichis, F., Hart, M.G., Griesbeck, M., Everett, H.L., Hassan, M., Baxter, A.E., Lindqvist, M., Miller, S.M., Soghoian, D.Z., Kavanagh, D.G., et al. (2014). High-throughput detection of miRNAs and gene-specific mRNA at the single-cell level by flow cytometry. *Nat. Commun.* *5*, 5641. <https://doi.org/10.1038/ncomms6641>.
44. Dufour, C., Richard, C., Pardons, M., Massanella, M., Ackaoui, A., Murrell, B., Routy, B., Thomas, R., Routy, J.P., Fromentin, R., and Chomont, N. (2023). Phenotypic characterization of single CD4+ T cells harboring genetically intact and inducible HIV genomes. *Nat. Commun.* *14*, 1115. <https://doi.org/10.1038/s41467-023-36772-x>.
45. Strazza, M., and Mor, A. (2017). Consider the chemokines: a review of the interplay between chemokines and T cell subset function. *Discov. Med.* *24*, 31–39.
46. Barczyk, M., Carracedo, S., and Gullberg, D. (2010). Integrins. *Cell Tissue Res.* *339*, 269–280. <https://doi.org/10.1007/s00441-009-0834-6>.
47. Becht, E., McInnes, L., Healy, J., Dutertre, C.-A., Kwok, I.W.H., Ng, L.G., Ginhoux, F., and Newell, E.W. (2018). Dimensionality reduction for

- visualizing single-cell data using UMAP. *Nat. Biotechnol.* 37, 38–44. <https://doi.org/10.1038/nbt.4314>.
48. Levine, J.H., Simonds, E.F., Bendall, S.C., Davis, K.L., Amir el, A.D., Tadmor, M.D., Litvin, O., Fienberg, H.G., Jager, A., Zunder, E.R., et al. (2015). Data-driven phenotypic dissection of AML reveals progenitor-like cells that correlate with prognosis. *Cell* 162, 184–197. <https://doi.org/10.1016/j.cell.2015.05.047>.
 49. Abdel-Mohsen, M., Kuri-Cervantes, L., Grau-Exposito, J., Spivak, A.M., Nell, R.A., Tomescu, C., Vadrevu, S.K., Giron, L.B., Serra-Peinado, C., Genescà, M., et al. (2018). CD32 is expressed on cells with transcriptionally active HIV but does not enrich for HIV DNA in resting T cells. *Sci. Transl. Med.* 10, eaar6759. <https://doi.org/10.1126/scitranslmed.aa6759>.
 50. Morou, A., Brunet-Ratnasingham, E., Dubé, M., Charlebois, R., Mercier, E., Darko, S., Brassard, N., Nganou-Makamdop, K., Arumugam, S., Gendron-Lepage, G., et al. (2019). Altered differentiation is central to HIV-specific CD4⁺ T cell dysfunction in progressive disease. *Nat. Immunol.* 20, 1059–1070. <https://doi.org/10.1038/s41590-019-0418-x>.
 51. Niessi, J., Baxter, A.E., Mendoza, P., Jankovic, M., Cohen, Y.Z., Butler, A.L., Lu, C.-L., Dubé, M., Shimeliovich, I., Gruell, H., et al. (2020). Combination anti-HIV-1 antibody therapy is associated with increased virus-specific T cell immunity. *Nat. Med.* 26, 222–227. <https://doi.org/10.1038/s41591-019-0747-1>.
 52. Nayrac, M., Dubé, M., Sannier, G., Nicolas, A., Marchitto, L., Tastet, O., Tauzin, A., Brassard, N., Lima-Barbosa, R., Beaudoin-Bussièrès, G., et al. (2022). Temporal associations of B and T cell immunity with robust vaccine responsiveness in a 16-week interval BNT162b2 regimen. *Cell Rep.* 39, 111013. <https://doi.org/10.1016/j.celrep.2022.111013>.
 53. Becattini, S., Latorre, D., Mele, F., Foglierini, M., De Gregorio, C., Cassotta, A., Fernandez, B., Kelderman, S., Schumacher, T.N., Corti, D., et al. (2015). T cell immunity. Functional heterogeneity of human memory CD4⁺ T cell clones primed by pathogens or vaccines. *Science* 347, 400–406. <https://doi.org/10.1126/science.1260668>.
 54. Morita, R., Schmitt, N., Bentebibel, S.-E., Ranganathan, R., Bourdery, L., Zurawski, G., Foucat, E., Dullaers, M., Oh, S., Sabzghabaei, N., et al. (2011). Human blood CXCR5(+)CD4(+) T cells are counterparts of T follicular cells and contain specific subsets that differentially support antibody secretion. *Immunity* 34, 108–121. <https://doi.org/10.1016/j.immuni.2010.12.012>.
 55. Grau-Expósito, J., Luque-Ballesteros, L., Navarro, J., Curran, A., Burgos, J., Ribera, E., Torrella, A., Planas, B., Badía, R., Martin-Castillo, M., et al. (2019). Latency reversal agents affect differently the latent reservoir present in distinct CD4⁺ T subpopulations. *PLoS Pathog.* 15, e1007991. <https://doi.org/10.1371/journal.ppat.1007991>.
 56. Sodroski, J., Rosen, C., Wong-Staal, F., Salahuddin, S.Z., Popovic, M., Arya, S., Gallo, R.C., and Haseltine, W.A. (1985). trans-acting transcriptional regulation of human T-cell leukemia virus type III long terminal repeat. *Science* 227, 171–173. <https://doi.org/10.1126/science.2981427>.
 57. Ho, Y.C., Shan, L., Hosmane, N.N., Wang, J., Laskey, S.B., Rosenbloom, D.I., Lai, J., Blankson, J.N., Siliciano, J.D., and Siliciano, R.F. (2013). Replication-competent noninduced proviruses in the latent reservoir increase barrier to HIV-1 cure. *Cell* 155, 540–551. <https://doi.org/10.1016/j.cell.2013.09.020>.
 58. Einkauf, K.B., Lee, G.Q., Gao, C., Sharaf, R., Sun, X., Hua, S., Chen, S.M., Jiang, C., Lian, X., Chowdhury, F.Z., et al. (2019). Intact HIV-1 proviruses accumulate at distinct chromosomal positions during prolonged antiretroviral therapy. *J. Clin. Invest.* 129, 988–998. <https://doi.org/10.1172/JCI124291>.
 59. Kwon, K.J., Timmons, A.E., SenGupta, S., Simonetti, F.R., Zhang, H., Hoh, R., Deeks, S.G., Siliciano, J.D., and Siliciano, R.F. (2020). Different human resting memory CD4⁺ T cell subsets show similar low inducibility of latent HIV-1 proviruses. *Sci. Transl. Med.* 12, eaax6795. <https://doi.org/10.1126/scitranslmed.aax6795>.
 60. Clark, I.C., Mudvari, P., Thaploo, S., Smith, S., Abu-Laban, M., Hamouda, M., Theberge, M., Shah, S., Ko, S.H., Pérez, L., et al. (2023). HIV silencing and cell survival signatures in infected T cell reservoirs. *Nature* 614, 318–325. <https://doi.org/10.1038/s41586-022-05556-6>.
 61. Sun, W., Gao, C., Hartana, C.A., Osborn, M.R., Einkauf, K.B., Lian, X., Bone, B., Bonheur, N., Chun, T.W., Rosenberg, E.S., et al. (2023). Phenotypic signatures of immune selection in HIV-1 reservoir cells. *Nature* 614, 309–317. <https://doi.org/10.1038/s41586-022-05538-8>.
 62. Chomont, N., El-Far, M., Ancuta, P., Trautmann, L., Procopio, F.A., Yassine-Diab, B., Boucher, G., Boulassel, M.R., Ghattas, G., Brechley, J.M., et al. (2009). HIV reservoir size and persistence are driven by T cell survival and homeostatic proliferation. *Nat. Med.* 15, 893–900. <https://doi.org/10.1038/nm.1972>.
 63. Wang, Z., Gurule, E.E., Brennan, T.P., Gerold, J.M., Kwon, K.J., Hosmane, N.N., Kumar, M.R., Beg, S.A., Capoferri, A.A., Ray, S.C., et al. (2018). Expanded cellular clones carrying replication-competent HIV-1 persist, wax, and wane. *Proc. Natl. Acad. Sci. USA* 115, E2575–E2584. <https://doi.org/10.1073/pnas.1720665115>.
 64. Hosmane, N.N., Kwon, K.J., Bruner, K.M., Capoferri, A.A., Beg, S., Rosenbloom, D.I., Keele, B.F., Ho, Y.-C., Siliciano, J.D., and Siliciano, R.F. (2017). Proliferation of latently infected CD4⁺ T cells carrying replication-competent HIV-1: potential role in latent reservoir dynamics. *J. Exp. Med.* 214, 959–972. <https://doi.org/10.1084/jem.20170193>.
 65. Mendoza, P., Jackson, J.R., Oliveira, T.Y., Gaebler, C., Ramos, V., Caskey, M., Jankovic, M., Nussenzweig, M.C., and Cohn, L.B. (2020). Antigen-responsive CD4⁺ T cell clones contribute to the HIV-1 latent reservoir. *J. Exp. Med.* 217, e20200051. <https://doi.org/10.1084/jem.20200051>.
 66. Buzon, M.J., Sun, H., Li, C., Shaw, A., Seiss, K., Ouyang, Z., Martin-Gayo, E., Leng, J., Henrich, T.J., Li, J.Z., et al. (2014). HIV-1 persistence in CD4⁺ T cells with stem cell-like properties. *Nat. Med.* 20, 139–142. <https://doi.org/10.1038/nm.3445>.
 67. Lee, G.Q., Orlova-Fink, N., Einkauf, K., Chowdhury, F.Z., Sun, X., Harrington, S., Kuo, H.-H., Hua, S., Chen, H.-R., Ouyang, Z., et al. (2017). Clonal expansion of genome-intact HIV-1 in functionally polarized Th1 CD4⁺ T cells. *J. Clin. Invest.* 127, 2689–2696. <https://doi.org/10.1172/JCI93289>.
 68. Jaafoura, S., de Goër de Herve, M.G., Hernandez-Vargas, E.A., Hendel-Chavez, H., Abdoh, M., Mateo, M.C., Krzysiek, R., Merad, M., Seng, R., Tardieu, M., et al. (2014). Progressive contraction of the latent HIV reservoir around a core of less-differentiated CD4⁺ memory T cells. *Nat. Commun.* 5, 5407. <https://doi.org/10.1038/ncomms6407>.
 69. Gosselin, A., Wiche Salinas, T.R., Planas, D., Wacleche, V.S., Zhang, Y., Fromentin, R., Chomont, N., Cohen, É.A., Shacklett, B., Mehraj, V., et al. (2017). HIV persists in CCR6+CD4⁺ T cells from colon and blood during antiretroviral therapy. *AIDS* 31, 35–48. <https://doi.org/10.1097/QAD.0000000000001309>.
 70. Pardons, M., Fromentin, R., Pagliuzza, A., Routy, J.P., and Chomont, N. (2019). Latency-reversing agents induce differential responses in distinct memory CD4⁺ T cell subsets in individuals on antiretroviral therapy. *Cell Rep.* 29, 2783–2795.e5. <https://doi.org/10.1016/j.celrep.2019.10.101>.
 71. Banga, R., Procopio, F.A., Ruggiero, A., Noto, A., Ohmiti, K., Cavassini, M., Corpataux, J.-M., Paxton, W.A., Pollakis, G., and Perreau, M. (2018). Blood CXCR3⁺ CD4⁺ T cells are enriched in inducible replication competent HIV in aviremic antiretroviral therapy-treated individuals. *Front. Immunol.* 9, 144. <https://doi.org/10.3389/fimmu.2018.00144>.
 72. Perreau, M., Savoye, A.L., De Crignis, E., Corpataux, J.M., Cubas, R., Haddad, E.K., De Leval, L., Graziosi, C., and Pantaleo, G. (2013). Follicular helper T cells serve as the major CD4⁺ T cell compartment for HIV-1 infection, replication, and production. *J. Exp. Med.* 210, 143–156. <https://doi.org/10.1084/jem.20121932>.
 73. Monteiro, P., Gosselin, A., Wacleche, V.S., El-Far, M., Said, E.A., Kared, H., Grandvaux, N., Boulassel, M.R., Routy, J.-P., and Ancuta, P. (2011). Memory CCR6+CD4⁺ T cells are preferential targets for productive HIV type 1 infection regardless of their expression of integrin β7. *J. Immunol.* 186, 4618–4630. <https://doi.org/10.4049/jimmunol.1004151>.

74. Estes, J.D., Kityo, C., Ssali, F., Swainson, L., Makamdop, K.N., Del Prete, G.Q., Deeks, S.G., Luciw, P.A., Chipman, J.G., Beilman, G.J., et al. (2017). Defining total-body AIDS-virus burden with implications for curative strategies. *Nat. Med.* **23**, 1271–1276. <https://doi.org/10.1038/nm.4411>.
75. Telwatte, S., Lee, S., Somsouk, M., Hatano, H., Baker, C., Kaiser, P., Kim, P., Chen, T.H., Milush, J., Hunt, P.W., et al. (2018). Gut and blood differ in constitutive blocks to HIV transcription, suggesting tissue-specific differences in the mechanisms that govern HIV latency. *PLoS Pathog.* **14**, e1007357. <https://doi.org/10.1371/journal.ppat.1007357>.
76. Stevenson, E.M., Ward, A.R., Truong, R., Thomas, A.S., Huang, S.-H., Dilling, T.R., Terry, S., Bui, J.K., Mota, T.M., Danesh, A., et al. (2021). HIV-specific T cell responses reflect substantive in vivo interactions with antigen despite long-term therapy. *JCI Insight* **6**, e142640. <https://doi.org/10.1172/jci.insight.142640>.
77. Huang, S.H., Ren, Y., Thomas, A.S., Chan, D., Mueller, S., Ward, A.R., Patel, S., Bollard, C.M., Cruz, C.R., Karandish, S., et al. (2018). Latent HIV reservoirs exhibit inherent resistance to elimination by CD8+ T cells. *J. Clin. Invest.* **128**, 876–889. <https://doi.org/10.1172/JCI97555>.
78. Ren, Y., Huang, S.H., Patel, S., Alberto, W.D.C., Magat, D., Ahimovic, D., Macedo, A.B., Durga, R., Chan, D., Zale, E., et al. (2020). BCL-2 antagonism sensitizes cytotoxic T cell-resistant HIV reservoirs to elimination ex vivo. *J. Clin. Invest.* **130**, 2542–2559. <https://doi.org/10.1172/JCI132374>.
79. Jiang, S., Chan, C.N., Rovira-Clavé, X., Chen, H., Bai, Y., Zhu, B., McCaffrey, E., Greenwald, N.F., Liu, C., Barlow, G.L., et al. (2022). Combined protein and nucleic acid imaging reveals virus-dependent B cell and macrophage immunosuppression of tissue microenvironments. *Immunity* **55**, 1118–1134.e8. <https://doi.org/10.1016/j.immuni.2022.03.020>.
80. Imamichi, H., Dewar, R.L., Adelsberger, J.W., Rehm, C.A., O'Doherty, U., Paxinos, E.E., Fauci, A.S., and Lane, H.C. (2016). Defective HIV-1 proviruses produce novel protein-coding RNA species in HIV-infected patients on combination antiretroviral therapy. *Proc. Natl. Acad. Sci. USA* **113**, 8783–8788. <https://doi.org/10.1073/pnas.1609057113>.
81. Einkauf, K.B., Osborn, M.R., Gao, C., Sun, W., Sun, X., Lian, X., Parsons, E.M., Gladkov, G.T., Seiger, K.W., Blackmer, J.E., et al. (2022). Parallel analysis of transcription, integration, and sequence of single HIV-1 proviruses. *Cell* **185**, 266–282.e15. <https://doi.org/10.1016/j.cell.2021.12.011>.
82. Vandergeeten, C., Fromentin, R., Merlini, E., Lawani, M.B., DaFonseca, S., Bakeman, W., McNulty, A., Ramgopal, M., Michael, N., Kim, J.H., et al. (2014). Cross-clade ultrasensitive PCR-based assays to measure HIV persistence in large-cohort studies. *J. Virol.* **88**, 12385–12396. <https://doi.org/10.1128/JVI.00609-14>.
83. Baxter, A.E., Niessl, J., Morou, A., and Kaufmann, D.E. (2017). RNA flow cytometric FISH for investigations into HIV immunology, vaccination and cure strategies. *AIDS Res. Ther.* **14**, 40. <https://doi.org/10.1186/s12981-017-0171-x>.
84. Dubé, M., and Kaufmann, D.E. (2022). Single-cell multiparametric analysis of rare HIV-infected cells identified by duplexed RNAflow-FISH. *Methods Mol. Biol.* **2407**, 291–313. https://doi.org/10.1007/978-1-0716-1871-4_20.
85. Brunet-Ratnasingham, E., Morou, A., Dubé, M., Niessl, J., Baxter, A.E., Tastet, O., Brassard, N., Ortega-Delgado, G., Charlebois, R., Freeman, G.J., et al. (2022). Immune checkpoint expression on HIV-specific CD4+ T cells and response to their blockade are dependent on lineage and function. *EBioMedicine* **84**, 104254. <https://doi.org/10.1016/j.ebiom.2022.104254>.
86. Quintelier, K., Couckuyt, A., Emmaneel, A., Aerts, J., Saeys, Y., and Van Gassen, S. (2021). Analyzing high-dimensional cytometry data using FlowSOM. *Nat. Protoc.* **16**, 3775–3801. <https://doi.org/10.1038/s41596-021-00550-0>.

STAR★METHODS

KEY RESOURCES TABLE

REAGENT or RESOURCE	SOURCE	IDENTIFIER
Antibodies		
UCHT1 (BUV395) [Human anti-CD3]	BD Biosciences	Cat#563546; Lot:9058566; RRID:AB_2744387
UCHT1 (BUV496) [Human anti-CD3]	BD Biosciences	Cat#612941; Lot:1022424; RRID:AB_2870222
L200 (BV711) [Human anti-CD4]	BD Biosciences	Cat#563913; Lot:03000025; RRID:AB_2738484
SK3 (BB630) [Human anti-CD4]	BD Biosciences	Cat#624294 CUSTOM; Lot:0289566
RPA-T8 (BV570) [Human anti-CD8]	Biolegend	Cat#301037; Lot:B281322; RRID:AB_10933259
M5E2 (BUV805) [Human anti-CD14]	BD Biosciences	Cat#612902; Lot:0262150; RRID:AB_2870189
M5E2 (BV480) [Human anti-CD14]	BD Biosciences	Cat#746304; Lot : 9133961; RRID:AB_2743629
3G8 (BV650) [Human anti-CD16]	Biolegend	Cat#302042; Lot:B323847; RRID:AB_2563801
HIB19 (APC-eFluor780) [Human anti-CD19]	Thermo Fisher Scientific	Cat#47-0199; Lot:2145095; RRID:AB_1582231
HIB19 (BV480) [Human anti-CD19]	BD Biosciences	Cat#746457; Lot:1021649; RRID:AB_2743759
HI100 (PerCP Cy5.5) [Human anti-CD45RA]	BD Biosciences	Cat#563429; Lot:8332746; RRID:AB_2738199
NCAM16.2 (BUV737) [Human anti-CD56]	BD Biosciences	Cat#564448; Lot:8288818; RRID:AB_2744432
FN50 (PerCP-eFluor710) [Human anti-CD69]	Thermo Fisher Scientific	Cat#46-0699-42; Lot:1920361; RRID:AB_2573694
FN50 (BV650) [Human anti-CD69]	Biolegend	Cat# 310934; Lot:B303462; RRID:AB_2563158
H4A3 (BV786) [Human anti-CD107A]	BD Biosciences	Cat#563869; Lot:8144866; RRID:AB_2738458
ACT35 (APC) [Human anti-CD134 (OX40)]	BD Biosciences	Cat#563473; Lot:1015537; RRID:AB_2738230
4B4-1 (PE-Dazzle 594) [Human anti-CD137 (4-1BB)]	Biolegend	Cat# 309826; Lot:B253152; RRID:AB_2566260
TRAP1 (BV421) [Human anti-CD154 (CD40L)]	BD Biosciences	Cat#563886; Lot:9037850; RRID:AB_2738466
TRAP1 (PE) [Human anti-CD154 (CD40L)]	BD Biosciences	Cat#555700; Lot:7086896; RRID:AB_396050
J25D4 (BV421) [Human anti-CD185 (CXCR5)]	Biolegend	Cat# 356920; Lot:B325837; RRID:AB_2562303
B27 (PECy7) [Human anti-IFN- γ]	BD Biosciences	Cat#557643; Lot:8256597; RRID:AB_396760
MQ1-17H12 (PE-Dazzle594) [Human anti-IL-2]	Biolegend	Cat#500344; Lot:B2261476; RRID:AB_2564091
JES3-9D7 (PE) [Human anti-IL-10]	BD Biosciences	Cat#554498; Lot:8198773; RRID:AB_395434
eBio64CAP17 (eFluor660) [Human anti-IL-17A]	Thermo Fisher Scientific	Cat#50-7179-42; Lot:2151998; RRID:AB_11149126
Mab11 (Alexa Fluor 488) [Human anti-TNF- α]	Biolegend	Cat#502915; Lot:B285221; RRID:AB_493121
Mab11 (APC) [Human anti-TNF- α]	BD Biosciences	Cat#562084 Lot: 0350627 RRID:AB_10893226
LIVE/DEAD Fixable dead cell	Thermo Fisher Scientific	L34960
Biological samples		
SARS-CoV-2 naïve donor blood samples	N/A	N/A
SARS-CoV-2 prior infection donor blood samples	N/A	N/A
Chemicals, peptides, and recombinant proteins		
PepMix™ SARS-CoV-2 (Spike Glycoprotein)	JPT	Cat#PM-WCPV-S-1
Staphylococcal Enterotoxin B (SEB)	Toxin technology	Cat#BT202
Software and algorithms		
Flow Jo v10.8.0	Flow Jo	https://www.flowjo.com
GraphPad Prism v8.4.1	GraphPad	https://www.graphpad.com
R studio v4.1.0	R studio	https://rstudio.com
R codes scripted	Github	https://github.com/otastet/Nayrac_et_al
Deposited data		
Sequence number		GenBank accession number
PWH9_L3p1_A2_C0_434		GenBank : OR105517

(Continued on next page)

Continued

REAGENT or RESOURCE	SOURCE	IDENTIFIER
PWH5_L2p3_A9_PCR2_G9_C0_455		GenBank : OR105518
PWH5_L2p2_F6_C0_290		GenBank : OR105519
PWH5_L2p2_E10_C0_386		GenBank : OR105520
PWH5_L2p2_E9_PCR2_E9_C0_454		GenBank : OR105521
PWH5_L2p2_E3_C0_463		GenBank : OR105522
PWH5_L2p2_D10_C0_432		GenBank : OR105523
PWH5_L2p1_C12_PCR2_C12_C0_440		GenBank : OR105524
PWH5_L2p1_C10_C0_473		GenBank : OR105525
PWH5_L2p1_C6_PCR2_C6_C0_474		GenBank : OR105526
PWH5_L2p1_B7_C0_325		GenBank : OR105527
PWH5_L2p1_B4_C0_391		GenBank : OR105528
PWH5_L2p1_A10_C0_341		GenBank : OR105529
PWH3_L1p3_B11_C0_402		GenBank : OR105530
PWH3_L1p3_A5_C0_417		GenBank : OR105531
PWH3_L1p3_A3_C0_418		GenBank : OR105532
PWH3_L1p2_H12_C0_390		GenBank : OR105533
PWH3_L1p2_H4_C0_378		GenBank : OR105534
PWH3_L1p2_G5_C0_392		GenBank : OR105535
PWH3_L1p2_F2_C0_412		GenBank : OR105536
PWH3_L1p2_D12_C0_394		GenBank : OR105537
PWH3_L1p2_D3_C0_399		GenBank : OR105538
PWH3_L1p2_C11_C0_329		GenBank : OR105539
PWH3_L1p2_C8_C0_432		GenBank : OR105540
PWH3_L1p2_C2_C0_366		GenBank : OR105541
PWH3_L1p2_B10_C0_371		GenBank : OR105542
PWH3_L1p2_A10_C0_42		GenBank : OR105543
PWH3_L1p1_H7_C0_263		GenBank : OR105544
PWH3_L1p1_G3_C0_365_inversion		GenBank : OR105545
PWH3_L1p1_G1_C0_430		GenBank : OR105546
PWH3_L1p1_F7_C0_350		GenBank : OR105547
PWH3_L1p1_F3_C0_418_inversion		GenBank : OR105548
PWH3_L1p1_E12_C0_413		GenBank : OR105549
PWH3_L1p1_E10_C0_430		GenBank : OR105550
PWH3_L1p1_D9_C0_436		GenBank : OR105551
PWH3_L1p1_D8_C0_366		GenBank : OR105552
PWH3_L1p1_C6_C0_390		GenBank : OR105553
PWH3_L1p1_B5_C0_422		GenBank : OR105554
PWH3_L1p1_B4_C0_392		GenBank : OR105555
PWH3_L1p1_A6_C0_433		GenBank : OR105556

RESOURCE AVAILABILITY

Lead contact

Further information and requests for resources and reagents should be directed to and fulfilled by the lead contact, Daniel E. Kaufmann (daniel.kaufmann@chuv.ch).

Materials availability

All unique reagents generated during this study are available from the [lead contact](#) upon a material transfer agreement (MTA).

Data and code availability

- The published article includes all datasets generated and analyzed for this study.

- We developed R codes scripted to perform unsupervised analysis of B and T cells from SARS-CoV-2 naive and previously infected individuals. All original codes have been deposited at Github and are publicly available as of publication. URL link is listed in the [key resources table](#).
- Gen Bank accession codes for single-cell HIV sequences are provided in [Table S5](#).
- Any additional information required to reanalyze the data reported in this paper is available from the [lead contact](#) Author upon request (daniel.kaufmann@chuv.ch).

EXPERIMENTAL MODEL AND SUBJECT DETAILS

Ethics Statement

All work was conducted following the Declaration of Helsinki regarding informed consent and approval by an appropriate institutional board. Blood samples were obtained from donors who consented to participate in this research project at CHUM (CE13.019).

Participants and Samples

Leukaphereses were obtained from study participants at the McGill University Health Centre, Montreal, Quebec, Canada, and at Centre Hospitalier de l'Université de Montréal (CHUM), Quebec, Canada. The study was approved by the respective IRBs, and written informed consent was obtained from all participants before enrolment. Uninfected donors (UD) are free of HIV-1 infection. Treated subjects (ART) were on antiretrovirals with controlled viremia (<40 vRNA copies/mL). Participants' characteristics are summarized in [Table S1](#). PBMCs were isolated by the Ficoll density gradient method and stored in liquid nitrogen until use.

METHOD DETAILS

Total and integrated DNA measures

The quantifications of total and integrated HIV-1 DNA were determined as previously described.⁸²

CD4⁺ T cell preparation for HIV reservoir profiling

Frozen PBMCs were thawed in cold heat-inactivated Fetal Calf Serum (FCS; Seradigm) before CD4⁺ T-cells isolation. CD4⁺ T-cells were isolated by negative magnetic bead selection (StemCell). Purified CD4⁺ T cells were resuspended at 2x10⁶/mL in RPMI (Gibco by Life Technologies) supplemented with penicillin/streptomycin (Gibco by Life Technologies), 10% heat-inactivated FCS, and ARV (Maraviroc [10μM] + Raltegravir [0.2μM] + Tenofovir [5μM]) + Emtricitabine [10μM] and seeded into 24-well plates (all obtained through the NIH AIDS Reagent Program). After a rest of 2h at 37°C, 5% CO₂, the cells were either left unstimulated or stimulated with PMA/ionomycin (162 nM PMA, 705 nM Ionomycin, Sigma) for 15-h. Alternatively, cells were either left unstimulated or stimulated with 30nM panobinostat (Selleck Chem) complemented with 25nM ingenol-3-angelate (Sigma). 10-15x10⁶ purified CD4⁺ T-cells were used per condition.

HIV-1 RNAflow-FISH assay

The HIV-1 RNAflow-FISH assay was performed as previously described and per the manufacturer's instructions.^{8,9,83,84} All buffers and fixation reagents were provided with the kit, except flow cytometry staining (1% FCS/PBS). Briefly, negatively purified CD4⁺ T cells were harvested after stimulation and stained first with Fixable Viability Dye (20 min, 4°C, Fixable LiveDead, eBioscience), FcR blocked, followed by a mix containing a brilliant stain buffer (BD Biosciences) and the surface markers for memory (CD45RA) and gut homing (integrin β7, CD103) phenotype, activation markers (HLA-DR, ICOS) and inhibitory checkpoint (PD-1) as well as for CD4⁺ T-cells detection (CD3 and CD4) and CD8/NK/B cells and macrophages exclusions (CD8, CD56, CD14, CD19, CD16) (30 min, 4°C). Anti-CXCR5, CCR6, CCR4, CXCR3, CCR7 and CD27 were added at 37°C 15 min before stimulation to stain chemokine receptors. Samples were fixed, permeabilized, and labeled intracellularly for the activation marker Ki67 and the structural HIV-1 p24 protein with the anti-p24 clone KC57 antibody (30 min RT followed by 30 min 4°C, Beckman Coulter). HIV-1 RNA probing was performed using the PrimeFlow RNA Assay (ThermoFisher). HIV-1 RNA was labeled using HIV-1 gagRNA (20 pairs of "ZZ" probes), HIV-1 exonRNA (21 pairs of "ZZ" probes), and HIV-1 polRNA (6 pairs of "ZZ" probes) probe sets, all designed based on a consensus B HIV sequence. The probes were diluted 1:5 in diluent and hybridized to the target mRNAs for 2 hrs at 40°C. Samples were washed to remove excess probes and stored overnight in the presence of RNAsin. Signal amplification was achieved by sequential 1.5 hr at 40°C incubations with the pre-amplification and amplification mix. Amplified mRNAs were labeled with fluorescently tagged probes for 1h at 40°C. The complete list of antibodies used is presented in [Table S2](#) for the panel. Samples were acquired on a FACSymphony™ (BD Biosciences) and analyzed using FlowJo (BD, V10.8.0). Unspecific binding of the fluorescent-labeled branched probe in the multiplex kit can lead to a low level of false-positive background noise, which, if present, is detected across all the four channels corresponding to the types of labeled probes (AF488, AF594, AF647, AF750). To decrease background noise, we thus left the AF594 channel vacant and excluded false-positive events based on fluorescence in this channel before further gating. Gates were set on the HIV-uninfected donor control or unstimulated control where appropriate (See gating strategy, [Figure S1](#)). Because HIV

infection can downregulate CD4, and because RNAflow-FISH was performed on negatively purified CD4⁺ T cells, no CD4 gating was applied during the analysis. To calculate the frequency of vRNA⁺ cells per 10⁶, we directly used as the denominator the counts of cells after the dump exclusion gating.

Limiting Dilution Assay

CD4⁺ T cells were isolated from PBMC by negative selection using magnetic beads (StemCell). After 18h hours of resting, the cells were distributed in limiting dilutions in a 96-well plate, with 11 replicates for each of the following dilutions: 100000, 50000, 16667, 5556 cells per well. The plate was spun at 300xg for 5 min, and the cell pellets were resuspended in Lysis/Binding solution (Magmax 96 Total RNA Isolation Kit, Life Technologies). Ca-RNA was extracted in plate using Magmax 96 Total RNA Isolation Kit (Life Technologies) following manufacturer's instructions. A nested RT-qPCR was performed to amplify LTRgag caRNA for all the replicates of each dilution. A 1-step RT and pre-amplification step was carried out by adding 9uL of extracted RNA (corresponding to 18000, 9000, 3000 and 1000 cell-equivalent depending on the dilution) to a mix of 6.25uL of Taq-1-Path master mix (Applied Biosystems) and 800 nM of LTRgag specific primers.⁸² The PCR cycles were as follow: 15 min at 53°C, 2 min at 95°C, and 18 cycles of 15 s at 95°C and 2 min at 60°C. The pre-amplified product was used to perform a real-time PCR as previously described.⁸² Positive wells at each dilution were counted and the maximum likelihood method was used to calculate the frequency of cells with LTRgag RNA (<http://bioinf.wehi.edu.au/software/elda>).

Microscopy

CD4⁺ T cells from one uninfected and one ART-treated PWH were isolated, rested 2h and reactivated with LRA (30nM panobinostat (Selleck Chem) and 25nM ingenol-3-angelate (Sigma) for 15h. Cells were collected and stained with a viability dye (Fixable Live/Dead (eF780, eBioscience) and with antibodies against surface CD8, CD14 and CD19 (BV510). mRNA Flow FISH was performed as described above and sorted with a BD FACS Aria. Single, CD8/14/19- T cells were sorted into two populations based on *exonRNA* AF647 and *gagRNA* AF488 staining (Figure S2H). Prior to microscopy analysis, nuclei were stained (DAPI, 1ng/ml, 2 min RT), directly loaded in ibidi μ -Slide VI 0.4 microscopy chambers and imaged using a Zeiss Axio Observer.Z1 inverted spinning disk confocal microscope coupled to an Evolve camera (EMCCD, 512x512, 16bit, 1.2x adapter) and ZEN blue software (version 2012). Images were acquired with an alpha Plan-Apochromat 100x/1.46 Oil DIC (UV) M27 objective. Excitation was performed with a 639nm, a 488nm and a 405nm solid state lasers for AF647, AF488 and DAPI respectively. Emission was collected through Chroma filters: DBP 527/54 + 645/60 for AF488 and AF647 and a DBP 460/30 + 590/30 for DAPI. Z-stacks were performed to image whole cells with a step size of 0.220 μ m. Final resolution is 0.133 μ m x 0.133 μ m x 0.220 μ m in xyz. Brightfield images were acquired with the same modalities but with a LED white light illumination, no filter and without Zstack. Fiji was used for all image analysis and facilitate counting. DAPI staining was used to define the nuclear compartment and the "Find Maxima" command was used to identify and count HIV RNA foci.

Single-cell near full-length PCR

Unstimulated CD4⁺ T-cells from 3 ART-treated donors were stained in HIV-1 RNAflow-FISH assays using HIV-1 *gagRNA*, *exonRNA*, and *polRNA* probes. Single vRNA⁺ cells were sorted in 12-wells PCR strips containing 8 μ L of DirectPCR Lysis Reagent (Viagen Biotech) with 0.4mg/mL proteinase K. The PCR strips were subsequently incubated at 55°C for 1h for cell lysis followed by 15 min at 85°C to inactivate proteinase K. Single sorted cells were subjected to near full-length amplification using a modified FLIPS assay.^{9,44} HIV-1 genomes were pre-amplified using Invitrogen Platinum SuperFi II MasterMix with 0.2 μ M of each primer.⁴⁴ 30 μ L of PCR mix was added directly to the lysed cells for a 25 cycles 3-steps PCR protocol as recommended by the manufacturer. The pre-amplified products were diluted 1:3 with Tris-HCl 0.5 μ M pH 8.0 and subjected to a nested PCR with 5 μ L of pre-amplified product, 2X of Platinum SuperFi II PCR Mix and 0.2 μ M of each primer in a 30 μ L final volume.⁴⁴ This second amplification consists in 30 cycles and follows the manufacturer's instructions. The length of the sequences obtained were verified on a 0.8% agarose gel and the amplicons were individually barcoded for PacBio Sequel II sequencing (DNA Link, South Korea), The demultiplex barcodes analysis was powered by the Lima PacBio software v2.0.0. High-quality phased consensus sequences representing near full HIV-1 genome sequences with high fidelity and without reconstruction have been generated with the LAA PacBio algorithm v2.4.2. For each individual, sequences obtained were aligned using Multiple Alignment using Fast Fourier Transform (MAFFT) with strategy E-INS-i and Scoring matrix for nucleotide sequences of 1PAM/ k=2 (online <https://mafft.cbrc.jp/alignment/server/> or with Geneious Prime (v2021.1.1) plugging). Trees were built with iqtree2 using Maximum-Likelihood tree GTR+I+G model, with 1000 bootstraps, and then visualized with Figtree (v1.4.4). Clonality was evaluated with diversity of sequences in Geneious Prime, and sequences with 0 nucleotide difference were considered clonal. Integrity was assessed using both HIVDatabase QCtool (<https://www.hiv.lanl.gov/content/sequence/QC/index.html>) and ProseqIT (https://psd.cancer.gov/tools/pvs_annot.php). Finally, Psi defects were confirmed manually by visualization in Geneious Prime of this portion of the sequence. Genbank accession numbers for single-cell sequences are provided in Table S5.

Activation-induced marker (AIM) assay

The AIM assay was reported before.^{29,30,50,51} PBMCs were thawed and rested for 3h in 96-well flat-bottom plates in RPMI 1640 supplemented with HEPES, penicillin and streptomycin and 10% FBS. 2x10⁶ PBMCs and stimulated with Gag or Pol or Env or Nef peptide 15-mers pools (0.5 μ g/ml per peptide) spanning the complete amino acid sequence of each HIV protein (JPT) for 15h at 37 °C and 5% CO₂. CD40-blocking antibody was added to prevent CD40L downregulation following activation. In addition,

CXCR3, CCR6, and CXCR5 antibodies were added to the culture 15 min before stimulation. A DMSO-treated condition served as a negative control and *Staphylococcus enterotoxin B* SEB-treated condition (0.5 $\mu\text{g}/\text{ml}$) as a positive control. Cells were stained for viability dye for 20 min at 4 °C, FcR receptors were blocked using an FcR block antibody, and then surface markers (CD3, CD4, CD8, CD45RA, CD69, OX40, 41BB, CD40L, PD1, HLA-DR) (30 min, 4 °C). Abs used are listed in the [Table S3](#). Cells were fixed using 2% paraformaldehyde for 15 min at 4 °C before acquisition on Symphony cytometer (BD Biosciences). Analyses were performed using FlowJo v10.8.0 software.

Intracellular Cytokine Staining (ICS)

The previously described ICS assay was adapted to study HIV-specific T cells.^{29,51,85} PBMCs were thawed and rested for 2-h in RPMI 1640 medium supplemented with 10% FBS, Penicillin-Streptomycin (Thermo Fisher Scientific, Waltham, MA), and HEPES (Thermo Fisher Scientific, Waltham, MA). 1.7×10^6 PBMCs were stimulated with Gag or Pol or Env or Nef peptide pools (0.5 $\mu\text{g}/\text{ml}$ per peptide; JPT) for 15h at 37 °C and 5% CO₂. Cell stimulation was carried out for 6h at 5% CO₂ at 37 °C. Brefeldin A and monensin (BD Biosciences, San Jose, CA) was added 1h after stimulation. DMSO-treated cells served as a negative control and SEB as a positive control. Cells were stained for Aquavid viability marker (Thermo Fisher Scientific, Waltham, MA) for 20 min at 4 °C, then surface markers (CD4, CD3, CD8, CD14, CD19; 30 min, 4 °C), followed by intracellular Detection of cytokines (IFN γ , Il-2, and TNF- α) using the IC Fixation/Permeabilization kit (Thermo Fisher Scientific, Waltham, MA) according to the manufacturer's protocol before acquisition on a LSRII flow cytometer (BD Biosciences). Analysis was performed using FlowJo v10.8.0 software. Abs used are listed in [Table S4](#).

QUANTIFICATION AND STATISTICAL ANALYSIS

Statistical analysis

Symbols represent biologically independent samples from uninfected and HIV-infected under suppressive ART. Wilcoxon, Mann-Whitney, and Friedman with Dunn's post-test were generated using GraphPad Prism version 8.4.3 (GraphPad, San Diego, CA). P values <0.05 were considered significant. P values are indicated for each comparison assessed. Fold differences were calculated per participant, then median of these fold differences was calculated. Median values were used to generate donut charts. Each median value was normalized to obtain a total of 100%. For descriptive correlations, Spearman's R correlation coefficient was applied. For graphical representation on a log scale (but not for statistical tests), null values were arbitrarily set at the minimum values for each assay.

Software scripts and visualization

Graphics and pie charts were generated using GraphPad PRISM version 8.4.1 and ggplot2 (v3.3.3) in R (v4.1.0). Heat maps were generated in GraphPad PRISM version 8.4.1. Uniform manifold approximation and projection (UMAP) was performed using package M3C (v1.14.0) on gated FCS files loaded through the flowCore package (v2.4.0). For reservoir phenotyping, all vRNA⁺ events were loaded along with 3000 downsampled autologous CD4⁺ T cells per participant, for a total of 1,418 vRNA⁺ cells + 51,000 autologous CD4⁺ T cells. For the AIM analysis, samples were downsampled to a comparable 300 cells per peptide (Gag, Pol, Env and Pol) pool tested, therefore 1200 peptide-specific cells per participant, and a grand total of 20,400 HIV-specific cells. This number was chosen to avoid biases due to larger responses in certain participants. Scaling and logicle transformation of the flow cytometry data were applied using the FlowSOM⁸⁶ R package (v2.0.0). Clustering was achieved using Phenograph (v0.99.1) with the hyperparameter k (number of nearest neighbors) set to 150). R code scripted for this paper was adapted from https://github.com/otastet/Nayrac_et_al with the parameters described above. We obtained an initial 18 AIM⁺ clusters. After careful examination, we regrouped these clusters into 6 larger superclusters based on similar chemokine receptor expression. For vRNA⁺ and CD4⁺ T cell phenotyping, only participants with >5 events were analyzed.